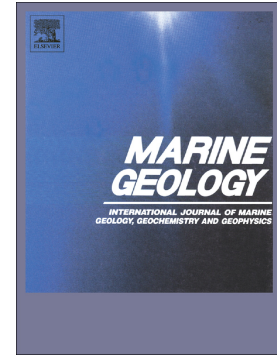


Accepted Manuscript

Evolution and development of Miocene “island dolostones” on Xisha Islands, China South Sea

Rui Wang, Kefu Yu, Brian Jones, Yinghui Wang, Jianxin Zhao, Yuexin Feng, Lizeng Bian, Shendong Xu, Tianlai Fan, Wei Jiang, Yu Zhang



PII: S0025-3227(17)30521-2
DOI: doi:[10.1016/j.margeo.2018.09.006](https://doi.org/10.1016/j.margeo.2018.09.006)
Reference: MARGO 5846
To appear in: *Marine Geology*
Received date: 31 October 2017
Revised date: 11 September 2018
Accepted date: 14 September 2018

Please cite this article as: Rui Wang, Kefu Yu, Brian Jones, Yinghui Wang, Jianxin Zhao, Yuexin Feng, Lizeng Bian, Shendong Xu, Tianlai Fan, Wei Jiang, Yu Zhang , Evolution and development of Miocene “island dolostones” on Xisha Islands, China South Sea. *Margo* (2018), doi:[10.1016/j.margeo.2018.09.006](https://doi.org/10.1016/j.margeo.2018.09.006)

This is a PDF file of an unedited manuscript that has been accepted for publication. As a service to our customers we are providing this early version of the manuscript. The manuscript will undergo copyediting, typesetting, and review of the resulting proof before it is published in its final form. Please note that during the production process errors may be discovered which could affect the content, and all legal disclaimers that apply to the journal pertain.

**Evolution and development of Miocene “island dolostones” on Xisha Islands, China South
Sea**

Rui Wang^a, Kefu Yu^{a,*}, Brian Jones^b, Yinghui Wang^a, Jianxin Zhao^c, Yuexin Feng^c, Lizeng
Bian^d, Shendong Xu^a, Tianlai Fan^a, Wei Jiang^a, Yu Zhang^a

^a Guangxi Laboratory on the Study of Coral Reefs in the South China Sea; Coral Reef Research
Center of China; School of Marine Sciences, Guangxi University, Nanning 530004, China

^b Department of Earth and Atmospheric Sciences, University of Alberta, Edmonton, Alberta, T5R
3C8, Canada

^c School of Earth Sciences, The University of Queensland, QLD4067, Australia

^d School of Earth Science and Engineering, Nanjing university, Nanjing 210093, China

*Corresponding author: Kefu Yu (kefuyu@scsio.ac.cn)

Abstract: On Xisha Islands, located in the South China Sea, the Neogene succession includes the unconformity-bounded Huangliu Formation that is 210.5 m thick in well CK-2 and formed almost entirely of dolostones. The diverse biota in the Huangliu Formation, which includes corals, algae, bivalves and foraminifera, indicates that the original carbonate sediments accumulated in water that was < 30 m deep. The dolostones are formed of various mixtures of low- and high-calcium calcian dolomite with limpid dolomite lining the walls of many cavities. The ^{18}O and ^{13}C stable isotopes suggest that dolomitization was mediated by slightly modified seawater. The $^{87}\text{Sr}/^{86}\text{Sr}$ ratios from the dolostones suggest that dolomitization took place ~9.4 and 2.3 Ma ago, with the age of dolomitization becoming progressively younger towards the top of the formation. “Island dolostones” like these, found on many islands throughout the Pacific Ocean and the Caribbean Sea, have commonly been linked to eustatic changes in sea-level with dolomitization taking place during lowstands, highstand, or transgressive phases. Data from the Huangliu Formation in well CK-2 suggests that dolomitization was associated with (semi-)continuous transgressive conditions that were controlled by the interaction of tectonic subsidence and eustatic changes in sea level.

Keywords: Island dolomite; Dolomitization; Sea-level change; Cenozoic; Xisha Islands

1. Introduction

Throughout the Pacific Ocean and Caribbean Sea there are numerous isolated islands that are characterized by thick successions of “island dolomite” (Budd, 1997). Prime examples include Grand Cayman (Jones and Luth, 2003; Ren and Jones, 2017, 2018), Kita-daito-jima (Suzuki et al., 2006), Mururoa (Aissaoui et al., 1986), Enewetak (Saller, 1984), Niue (Aharon et al., 1987; Wheeler et al., 1999) and the Bahamian Platform (Dawans and Swart, 1988; Swart and Melim, 2000; Vahrenkamp and Swart, 1994). Research on these successions has focused largely on resolution of the “dolomite problem” and explanation of how these thick successions of dolomite formed. It has been suggested that many of these island dolostones successions may have been developed through one or more episodes of dolomitization (Budd, 1997; Jones and Luth, 2003; Suzuki et al., 2006). Jones et al. (1984) and Pleydell et al. (1990), for example, argued that the dolostones in the Cayman Formation and Pedro Castle Formation on Grand Cayman formed during a single phase of dolomitization. Conversely, Ng (1990) argued that two phases of dolomitization had affected the Cayman Formation and Jones and Luth (2003) used the $^{87}\text{Sr}/^{86}\text{Sr}$ ratios of the dolostones to suggest that three phases of dolomitization affected this formation. On Kita-daito-jima three of four phases of dolomitization have been proposed (Suzuki et al., 2006),

Based on comparisons of $^{87}\text{Sr}/^{86}\text{Sr}$ ratios from many carbonate islands in Caribbean Sea and Pacific Ocean, Budd (1997, his Table 5, Fig. 19) suggested that global dolomitization events included “early” (0.70896 to 0.70901) and “late” (0.70905 to 0.70910) phases that could be divided into parts A, B, C, D, E, F, and G. In addition, Machel (2000) suggested that the $^{87}\text{Sr}/^{86}\text{Sr}$

data in Pleydell et al. (1990) exhibited too great a range to warrant attribution to a single phase of dolomitization. These conclusions tacitly assumed that each phase of dolomitization was a time-restricted “event” with a unique $^{87}\text{Sr}/^{86}\text{Sr}$ “signal” and that multiple phases of dolomitization should generate multimodal frequency histograms. Recent studies of dolomitization on the Grand Cayman and Cayman Brac (Jones and Luth, 2002, 2003; MacNeil and Jones, 2003; Zhao and Jones, 2012a; Ren and Jones, 2017) followed that premise.

Worldwide synchronicity in the timing of dolomitization has led to the suggestion that dolomitization may be related to eustatic changes in sea-level (Budd, 1997; Jones and Luth, 2003; Suzuki et al., 2006; Zhao and Jones, 2012a). Budd (1997), for example, suggested that stable sea-level positions (lowstand or highstand) may favor dolomitization because that would allow vast quantities of waters to circulate through the strata over a long-time period and supply the Mg needed for dolomitization to take place. The dolostones on Kita-daito-jima, for example, may have been formed during a lowstand (Suzuki et al. 2006). Conversely, Jones and Luth (2003) suggested that dolomitization on Grand Cayman may have been associated with a transgression.

On Xisha Islands, located in the South China Sea (Fig. 1), the Huangliu Formation (average 235 m thick) is formed of dolostones that are similar to island dolostones found on other islands. Previous studies suggested that these dolostones formed through the circulation of super hypersaline brine during the Messinian (Wei et al., 2007; Wei et al., 2008; Zhao, 2010; Wang et al., 2015; Xiu et al., 2017) or slightly evaporated seawater (Wang et al., 2018). Based largely on the petrographic and geochemical characteristics of the Huangliu Formation in well ChenKe-2 (CK-2) on Xisha Islands (Fig. 1), this study considers the type of fluid that mediated

dolomitization, uses the $^{87}\text{Sr}/^{86}\text{Sr}$ ratios to establish when dolomitization took place, and then compares the evolution of these dolostones with island dolostones found on other islands throughout the oceans of the world. Collectively, this information provides the basis for suggesting that the dolostones on Xisha Islands probably formed during a (semi-)continuous time-transgressive dolomitization process that resulted from the combined effects of tectonic subsidence and eustatic changes in sea level.

2. Geological setting

The Xisha Islands (Fig. 1A, B), also known as the Paracel Islands, are located in the northwest part of the South China Sea and encompass more than 40 islands and reefs. The Xisha Platform on which these islands are located is surrounded by basins and/or depressions with ocean waters that are > 1000 m deep (Wu et al., 2014). Today, this area receives 1300 to 2000 mm rainfall each year, and the annual average surface temperature of the seawater is 22 to 30 °C with a near-surface salinity of 33.14 to 34.24‰ (Shao et al., 2017a).

Over the last 30 years, six wells (Xiyong-1 (XY-1), Xishi-1 (XS-1), Xishi-2 (XS-2), Xichen-1 (XC-1), Xike-1 (XK-1, also named ZK-1), Chenke-2 (CK-2)) (Fig. 1C, D) have been drilled to various depths on the Xisha Islands. Two of these wells (XY-1, XK-1) penetrated the entire Cenozoic carbonate succession (up to 1257.2 m thick) before terminating in the Paleozoic or older metamorphic basement rocks (Fig. 2A) (Zhao, 2010; Shao et al., 2017a). Well CK-2, located on Chenhang Dao (Fig. 1C), penetrated volcanoclastic rocks at a depth of 877 m (Fig. 2A). Some 2D/3D seismic data show that the Xisha Platform was initiated on a basement high,

the Xisha Uplift (Fig. 2B), during the early Miocene (Wu et al., 2014). The Xisha Platform is formed of fault-bounded blocks (Fig. 2B) that developed during the Xisha Uplift (Wu et al., 2014). Available evidence indicates that carbonate deposition was initiated at the beginning of the Miocene and flourished throughout the middle Miocene before waning during the late Miocene as the platform was drowned and significantly reduced in size during Pliocene-Quaternary times (Zhao, 2010; Wu et al., 2014; Kuang et al., 2014; Shao et al., 2017a; Shao et al., 2017b).

The carbonate succession on the Xisha Platform (Fig. 3) is divided into the unconformity-bounded Sanya Formation, Meishan Formation, Huangliu Formation, Yinggehai Formation, and Ledong Formation (Zhao, 2010; Wu et al., 2014; Shao et al., 2017a; Shao et al., 2017b). The sedimentary facies and coral reef development (Zhao, 2010; Shao et al., 2017a, b; Wang et al., 2018) indicate that this succession encompasses two shallow-water cycles that are represented by (1) the Sanya Formation, Meishan Formation, and Huangliu Formation (Early Miocene to Late Miocene), and (2) the Yinggehai Formation to Ledong Formation (Pliocene to Pleistocene) (Fig. 3). Most of the dolostones are found in the Huangliu Formation, which is probably late Miocene in age (Zhao, 2010; Shao et al., 2017a, b; Wang et al., 2018).

The dolostones in the Huangliu Formation in wells XC-1, CK-2, XY-1, and XK-1 are 200.5 m (well XK-1) to 290 m (well XY-1) thick with an average thickness of 235 m (Fig. 4A). Apart from some dolomitic limestone beds in XK-1, the dolostones in the Huangliu Formation contain > 98% dolomite (Wei et al., 2007; Zhao, 2010; Wang et al., 2015; Wang et al., 2018). The basal unconformity of the Huangliu Formation separates the dolostones from the limestone of the

underlying Meishan Formation, whereas the upper bounding unconformity separates it from the overlying Yinggehai Formation (Wei et al., 2007; Zhao, 2010; Wang et al., 2015; Shao et al., 2017a; Wang et al., 2018). The dolostones in the Huangliu Formation from CK-2 are divided into four unconformity-bounded units that are herein labeled, in ascending order, as units 1, 2, 3, and 4 (Fig. 4B)

3. Methods

The dolostone samples used in this study came from the core from well CK-2. The petrography of the dolostones was established by standard thin-section techniques (126 samples), with all thin sections being stained with Alizarin Red-S solution. Fourteen polished thin sections were examined on a Cambridge Image Technology Ltd. (CITL) CCL 8200 MK4 cathodoluminescence system in the State Key Laboratory of Geological Processes and Mineral Resources, China University of Geosciences (Wuhan, China), which was operated at 10-15 kV beam and 400-500 mA beam current.

After the core from CK-2 had been washed to remove salt, 224 samples (30 to 50 g) were collected at 1 m intervals using a dental drill. After the samples were powdering in an agate mortar, they were used to determine mineral content, rare earth elements, carbon-oxygen isotopes, and $^{87}\text{Sr}/^{86}\text{Sr}$ ratios.

One hundred and three samples (ca. 2 m interval) were subjected to X-ray diffraction (XRD) analysis using a Rigaku Ultima IV XRD system with Cu K α radiation (from 25° to 38° 2 θ at 40 kV and 35 mA), which is located in the Guangxi Laboratory on the Study of Coral Reefs in the

South China Sea, Guangxi University, China. These analyses followed the protocol of Jones et al. (2001).

Two hundred and two samples were used to determine element content and rare earth elements in the Guangxi Laboratory on the Study of Coral Reefs in the South China Sea, Guangxi University, China. 40 mg samples were placed in a PTFE digestion tank, then mixed with 2 ml 1:10 HF-HNO₃ acid solution, and kept at a temperature of 180 °C on an electric heating plate for 24 h. After that, the sample was dried and 1ml H₂O and 1ml HNO₃ was added before being dissolved again at 180 °C on an electric heating plate for 12 h. Finally, a 2% HNO₃ solution was used to dissolve the sample before it was placed into a refrigerator at 4 °C prior to inductively coupled plasma mass spectrometry (ICP-MS) was used to analysis the samples.

One hundred and eighty-four samples for carbon and oxygen isotopes were analyzed in the Guangxi Laboratory on the Study of Coral Reefs in the South China Sea, Guangxi University, China. Powdered samples were reacted with 100% H₃PO₄ at 75 °C for 30 minutes before the CO₂ was extracted and analyzed on a Finnigan MAT-253 stable isotope mass spectrometer. The isotopic ratios are reported in the per mil (‰) convention and normalized to the Vienna Pee Dee Belemnite (V-PDB) using the GBW04405 standard ($\delta^{13}\text{C} = 0.57\text{‰}$; $\delta^{18}\text{O} = - 8.49\text{‰}$). Multiple measurements ($n = 15$) of this standard yielded a standard deviation of 0.05‰ for $\delta^{13}\text{C}$, and 0.08‰ for $\delta^{18}\text{O}$. In addition, ~20% of the samples underwent duplicate analyses in order to further test the accuracy of the results. The standard errors of each repeated measurements are < 0.05‰ for $\delta^{13}\text{C}$ and < 0.08‰ for $\delta^{18}\text{O}$.

The $^{87}\text{Sr}/^{86}\text{Sr}$ analyses, obtained from 25 samples (~10 m interval) of pure dolostones, were done at the Radiogenic Isotope Laboratory, University of Queensland. Samples were first washed with 0.25N acetic acid and then dissolved in 1N acetic acid prior to column chemistry using Sr-spec resin and was analyzed on a VG Sector-54 thermal ionization mass spectrometer. The certified value of modern seawater standard EN-1 is 0.709175. The raw strontium isotope ratio and instrumental precision (± 0.000015) for each sample was corrected to the NIST-987 value of 0.710248 so that the McArthur et al. (2001) LOWESS lookup curve could be used.

4. Results

4.1. Petrography

The Huangliu Formation in well CK-2 is formed of units 1, 2, 3, and 4 that are separated from each other by unconformities.

4.1.1. Unit 1

Unit 1 (434.5 to 519 m) is formed of tan, well-indurated medium to coarsely crystalline dolostones that are characterized by fabric-destructive textures. These dolostones are composed of interlocking anhedral to euhedral dolomite crystals (most 10 to 60 μm) and euhedral limpid dolomite crystals (most 30 to 140 μm long, up to 500 μm long) (Fig. 5A, B). Although most of the dolostones are characterized by fabric-destructive textures, fabric-retentive dolostones are present in the upper 20 m (434.5 to 454 m) of the unit. In unit 1, limpid dolomite crystals line the secondary pores (Fig. 5B) and cavities, and/or are found in small patches in the matrix dolomites

(Fig. 5C). Some of matrix dolomite crystals have cloudy centers that are encased by clear rims (Fig. 5D). As described by Budd (1997), the euhedral limpid dolomite crystals in the pores and cavities developed as cement, whereas most of the matrix is formed replacive dolomites. Mimetically replaced red algae fragments (Fig. 5B, E) and open biomolds (Fig. 5F) are rare in unit 1.

4.1.2. Units 2, 3, and 4

Units 2 (364 to 434.5 m), 3 (316 to 364 m), and 4 (308.5 to 316 m) are formed of grey, fine to medium crystalline dolostones that are characterized by fabric-retentive textures (Fig. 6), which contrast sharply with the fabric-destructive dolostones in unit 1.

The dolostones in the unit 2, 3, and 4 have matrices formed of interlocking finely crystalline anhedral to subhedral dolomite (< 30 μm long) and cavities that are lined or filled with euhedral limpid dolomite cements (20 to 60 μm long) (Fig. 6A-C). Many crystals in the matrix dolomite and limpid dolomite cements have dirty cores encased by clear rims (Fig. 6D). In some of the matrix dolomite crystals, preferential dissolution of the cores produced hollow crystals (Fig. 6D), some of which were subsequently filled with dolomite (Fig. 6D) to produce inside-out dolomite (cf., Jones, 2007). Although limpid dolomite cements are common in units 2, 3, and 4 in the Huangliu Formation (Fig. 6E), there are scattered dissolution molds that do not contain any cements (Fig. 6F).

The original fabrics of the precursor limestone are preserved to varying degrees in units 2, 3, and 4. Biofragments originally formed of Mg-calcite, including red algae, have been mimetically

preserved (Fig. 6G). In contrast, skeletons originally formed of aragonite (e.g., corals, gastropods, bivalves) have generally been dissolved with fossil-moldic porosity being formed (Fig. 6F).

Although originally formed of aragonite, many of the *Halimeda* plates were mimetically preserved (Fig. 6B, H). In rare cases, some of the original skeletal material is preserved (Fig. 6I).

The cathodoluminescence (CL) signatures of the dolostones in the units 2, 3, and 4 are different from those in unit 1 (Fig. 7). The finely crystalline dolostones in units 2, 3, and 4 are characterized by relatively dark, dull red CL with scattered bright spots (Fig. 7A) and dolomite cements that are zoned with dull red CL (Fig. 7A). In contrast, the dolostones in unit 1 are characterized by bright red CL (Fig. 7B) and the dolomite crystals that form the cements and matrix are characterized by CL zoning (Fig. 7B).

4.2. Major elements and dolomite stoichiometry

Except for the basal 2 m (517 to 519 m, intercalated limestone and dolostone), the dolostones in the Huangliu Formation in CK-2 contain 15 to 22 wt% MgO, (average 20 wt%), and 15 to 38 wt% CaO (average 31 wt%).

The dolostones in the Huangliu Formation of CK-2 are formed of various mixtures of low-calcium calcian dolomite (LCD) and high-calcium calcian dolomite (HCD) and variable average mol %CaCO₃ (hereafter referred to as %Ca, following Jones et al. (2001)) (Fig. 8A, B). The average %Ca in units 1, 2, 3, and 4 are similar with 55.3, 55.2, 55.7, and 56.2% respectively (Fig. 8). Overall, the succession is formed largely of HCD-dominated dolostones with an average %Ca = 55.4% (n = 103). On average, the percentage of HCD increases from 63.5%

HCD in unit 1, to 71.9% HCD in unit 2, to 84.7% in unit 3, and 100% in unit 4 (Fig. 8B).

Throughout the succession, %LCD tends to be highest just below the unconformities (Fig. 8B).

4.3. Oxygen and carbon isotopes

The dolostones in the Huangliu Formation from well CK-2 (184 samples) yielded $\delta^{18}\text{O}$ values from 2.0 to 4.7‰ (average 3.3‰) and $\delta^{13}\text{C}$ values from 1.0 to 3.0‰ (average 2.3‰) (Fig. 9A).

- Unit 1: the $\delta^{18}\text{O}$ values range from 2.0 to 4.5‰ (average 2.9‰, $n = 77$), and the $\delta^{13}\text{C}$ ranges from 1.9 to 2.7‰ (average 2.4‰, $n = 77$) (Fig. 9A).
- Unit 2: the $\delta^{18}\text{O}$ ranges from 2.4 to 4.7‰ (average 3.6‰, $n = 65$), and the $\delta^{13}\text{C}$ ranges from 2.0 to 3.0‰ (average 2.6‰, $n = 65$) (Fig. 9A).
- Unit 3: the $\delta^{18}\text{O}$ ranges from 2.1 to 4.2‰ (average 3.6‰, $n = 35$), and the $\delta^{13}\text{C}$ ranges from 1.0 to 2.4‰ (average 1.9‰, $n = 35$) (Fig. 9A).
- Unit 4: the $\delta^{18}\text{O}$ ranges from 2.8 to 3.9‰ (average 3.2‰, $n = 7$), and the $\delta^{13}\text{C}$ ranges from 1.5 to 2.8‰ (average 2.4‰, $n = 7$) (Fig. 9A).

There is no correlation between the oxygen and carbon isotopes (Fig. 9A). The $\delta^{18}\text{O}$ values of the dolomites of unit 1 (average 2.9‰) are slightly more negative than those from units 2, 3, and 4 (average 3.5, 3.6, and 3.2‰, respectively), whereas the dolomites of unit 3 have slightly more negative $\delta^{13}\text{C}$ values (average 2.0‰) than those in units 1, 2, and 4 (average 2.4, 2.6 and 2.4‰, respectively) (Fig. 9A).

The $\delta^{13}\text{C}$ values for units 1, 2, and 4 (364 to 520 m; 308.5 to 316 m) are generally between 2.4 and 2.6‰, whereas those from unit 3 (316 to 364 m), with values 2.0‰, are generally lower

(Fig. 10B). The $\delta^{18}\text{O}$ values in the upper part of unit 1 (434.5 to 475 m) are generally from 2.0 to 3.0‰, which are lower than those values (generally from 3.0 to 4.0‰) in other parts of the Huangliu Formation dolostones (308.5 to 434.5 m; 475 to 520 m) (Fig. 10B).

4.4. Sr distribution and strontium isotopes

The Sr content of the dolostones (Table 1) ranges from 88 to 417 ppm (average 233 ppm, $n = 25$). For unit 1, the range is 88 to 329 ppm (average 198 ppm, $n = 10$), whereas for unit 2 it is 189 to 417 ppm (average 299 ppm, $n = 8$), for unit 3 it is 134 to 320 ppm (average 236 ppm, $n = 5$), and for unit 4 it is 151 to 122 ppm (average 137 ppm, $n = 2$) (Table 1; Fig. 11A).

The dolostones from the Huangliu Formation in CK-2 (units 1 to 4) yielded $^{87}\text{Sr}/^{86}\text{Sr}$ ratios of 0.708898 to 0.709075 ($n = 25$) with an average of 0.708960 (average $2s = 0.00001$) (Table 1). In unit 1, the $^{87}\text{Sr}/^{86}\text{Sr}$ ratios range from 0.708898 to 0.708926 (average 0.708911, $n = 10$), whereas those from unit 2 range from 0.708926 to 0.708981 (average 0.708953, $n = 7$), those from unit 3 range from 0.708988 to 0.709048 (average 0.709029, $n = 5$) and those from unit 4 range from 0.709049 to 0.709075 (average 0.709062, $n = 2$) (Table 1; Fig. 11A). The correlation between $^{87}\text{Sr}/^{86}\text{Sr}$ values and the Sr contents of the dolomites from CK-2 is low (Fig. 11A).

In well CK-2, the $^{87}\text{Sr}/^{86}\text{Sr}$ ratios gradually increase towards the top of the Huangliu Formation (Fig. 12).

4.5. Rare earth elements

The total REE+Y in the dolostones of the Huangliu Formation from well CK-2 range from 1 to 40 ppm (average 9 ppm) with the REE patterns for units 1, 2, 3, and 4 being similar (Fig. 13).

All of the samples are heavy-REE (HREE) enriched (average DyN/SmN = 1.37, n = 202), with similar values in the units 1 (average DyN/SmN = 1.31, n = 79), 2 (DyN/SmN = 1.34, n = 67), 3 (average DyN/SmN = 1.46, n = 49), and slightly higher values in unit 4 (average DyN/SmN = 1.67, n = 7). Samples from units 3 and 4 have slightly lower Ce/Ce* values (average 0.44, n = 49; average 0.44, n = 7; respectively) than those from units 1 (average 0.62, n = 79) and 2 (average 0.65, n = 67). Most samples have high Y/Ho mass ratios between 0.86 and 2.99 (average 1.56, n = 202), with similar ratios in units 1 (average 1.59, n = 79), 2 (average 1.57, n = 67), 3 (average 1.49, n = 49), and 4 (average 1.63, n = 7).

The dolostones from the Huangliu Formation in CK-2 are characterized by typical seawater REE patterns with HREE enrichment (average DyN/SmN = 1.37), negative Ce anomalies (average Ce/Ce* = 0.58), high Y/Ho ratios (average = 1.56), and a La surplus when normalized to the Post-Archean Australian Shale (PAAS) (Taylor and McLennan, 1985) REE patterns (Fig.13).

4.6. Unconformities

The Huangliu Formation in well CK-2 is unconformity bounded (basal and upper) and includes three internal unconformities that are herein labeled A, B, and C for ease of reference (Fig. 4B). These unconformities, which record critical stages in the evolution of the succession, are based on the following characteristics:

- Basal Unconformity (519 m): This unconformity is delineated by the lithological change from the white/grey limestones of the Meishan Formation to the tan/yellow dolostones of the Huangliu Formation.

- Unconformity A (434.5 m): This unconformity is delineated by (a) a change from the tan/yellow dolostones in unit 1 to the white/gray dolostones of unit 2, (b) a change from fabric-retentive dolostones in unit 1 to fabric-destructive dolostones in unit 2, (c) an increase in $\delta^{18}\text{O}$ values from unit 1 (average 2.9‰) to unit 2 (average 3.5‰) (Fig. 10B), and (d) a decrease in the %LCD content from the top of unit 1 to the base of unit 2 (Fig. 8B).
- Unconformity B (364 m): This unconformity is highlighted by (a) dolostones below this unconformity are characterized by yellow-brown ferrous staining, (b) a change in the %LCD content (Fig. 8B), and (c) a decrease in the $\delta^{13}\text{C}$ values of the dolostones from unit 2 (average 2.6‰) to unit 3 (average 1.9‰) (Fig. 10B).
- Unconformity C (316 m): This unconformity is characterized by (a) yellow-brown ferrous staining of the underlying dolostones, (b) a change in the %LCD (Fig. 8B), and (c) an increase in $\delta^{13}\text{C}$ values from unit 3 (average 1.9‰) to unit 4 (average 2.4‰) (Fig. 10B)
- Upper Unconformity (308.5 m): This unconformity, which defines the upper boundary of the Huangliu Formation, is highlighted by (a) yellow-brown ferrous staining of the underlying dolostones and (b) an upward change from dolostones to intercalated limestone/dolostone (Fig. 4B).

5. Comparison with other main wells on Xisha Islands

Comparisons of the Huangliu Formation in well CK-2 with other wells drilled on the Xisha Islands (Wei et al., 2007; Wei et al., 2008; Zhao, 2010; Wang et al., 2015; Xiu et al., 2017; Shao

et al., 2017a,b; Wang et al., 2018) is, in some cases difficult, because of the variable nature of the samples (cuttings or core) and the variable descriptions of the successions. Well XC-1, located in the northwest corner of Chenghang Dao, is ~1 km northwest of well CK-2 (Fig. 1C). Wells XY-1 and XK-1, located on Yongxing Dao and Shi Dao, are ~80 km and ~81 km north-east of well CK-2, respectively (Fig. 1B, D). The successions in wells XC-1 and XK-1 were cored, whereas only cuttings are available from well XY-1 (Wei et al., 2007; Zhao, 2010; Wang et al., 2015).

5.1. Stratigraphy

In well XC-1, unconformities in the Huangliu Formation have been identified at depths of about 319, 351, 451, and 548 m (Wei et al., 2007; Zhao, 2010), whereas Wang et al. (2015) identified unconformities in well XK-1 at depths of about 370, 470, and 576.5 m (Fig. 4A). In contrast, Shao et al. (2017a) placed unconformities at depths of about 370, 425, 470, 480, 528, and 576.5 m in well XK-1. Given that only cuttings were available for well XY-1, only the exposure surfaces on the top (at depth of ~ 370 m) and the bottom (at depth of ~ 360 m) of Huangliu Formation were reported (Zhao, 2010).

The dolostones in well CK-2 are similar to those in well XC-1, but unlike those in well XK-1. In XC-1, the grey, fine to medium crystalline dolostones with fabric-retentive dolostones between the depths of 319 and 451 m (Wei et al., 2007; Zhao, 2010) are similar to the dolostones in units 2, 3, and 4 of well CK-2. In well XC-1, the brown to grey-yellow dolostones (Wei et al., 2007, 2008; Zhao, 2010) between 451 and 548 m appear similar to the dolostones that form unit

1 in well CK-2. Unit 1, as identified in well CK-2, does not seem to be reported in wells XK-1 and XY-1.

Compared to CK-2, the Huangliu Formation in well XC-1 can, on the basis of internal unconformities, be divided into: (1) unit 1 (ca. 451 to 548 m) with brown to grey-yellow dolostones; (2) unit 2 (ca. 351 to 451 m) with gray fine to medium crystalline dolostones, and (3) unit 3 (ca. 319 to 351m) formed of gray fine to medium crystalline dolostones that may be equivalent to units 3 and 4 in CK-2. For well XK-1, given the different numbers of internal unconformities reported by Wang et al. (2015) and Shao et al. (2017a), two units or five units can be identified. For well XY-1, for which only cuttings are available, no internal unconformities were identified in the Huangliu Formation (Zhao, 2010). Thus, it is difficult to correlate the unconformities in the Huangliu Formation in wells XK-1 and XY-1 with the successions in well CK-2.

5.2. Oxygen and carbon isotopes

The dolostones in the Huangliu Formation in wells XC-1 and XK-1, as reported by Zhao (2010) and Wang et al. (2015), have $\delta^{18}\text{O}$ and $\delta^{13}\text{C}$ values similar to those from CK-2 (Fig. 9B). For the dolostones from XC-1, the $\delta^{18}\text{O}$ ranges from 1.1 to 5.2‰ (average 2.7‰, n = 52), and the $\delta^{13}\text{C}$ ranges from 1.8 to 3.2‰ (average 2.5‰, n = 52). For the dolostones from XK-1, the $\delta^{18}\text{O}$ ranges from 2.3 to 5.1‰ (average 3.7‰, n = 89), and the $\delta^{13}\text{C}$ ranges from 1.2 to 3.1‰ (average 2.4‰, n = 89). As for well CK-2, the oxygen and carbon isotopes of the dolostones from XC-1 and XK-1 do not co-vary (Fig. 9B). The vertical trend of the $\delta^{18}\text{O}$ and $\delta^{13}\text{C}$ values for well XC-1

are similar to those from CK2 (Fig. 10A). In XC-1, the $\delta^{13}\text{C}$ values are relatively stable between 2.3 and 3.0‰, whereas there are no obvious low values of $\delta^{18}\text{O}$ in the upper part of unit 1 (ca. 451 to 471 m) as in CK-2. For the dolostones from XK-1, the $\delta^{13}\text{C}$ values slightly decrease upward from 3 to 2‰ in the Huangliu Formation, whereas the $\delta^{18}\text{O}$ values range from 2.5 to 4.6‰ (Fig. 10C). In wells XC-1 and XK-1, there are no clear correlations between the $\delta^{18}\text{O}$ and $\delta^{13}\text{C}$ values and depth (Fig. 10A, C).

5.3. Sr distribution and strontium isotopes

In XC-1, the Sr content of the dolostones range from 129 to 205 ppm (average 176 ppm, $n = 28$), as reported by Wei et al. (2007), are lower than these in well CK-2 (average 233 ppm, $n = 25$) (Table 1; Fig. 11A, B). The Sr values for unit 1 are 151 to 200 ppm (average 183 ppm, $n = 17$), whereas for unit 2 the Sr ranges from 139 to 205 ppm (average 166 ppm, $n = 11$) (Fig. 11B).

The $^{87}\text{Sr}/^{86}\text{Sr}$ ratios of the dolostones from the Huangliu Formation in XC-1 (Wei et al., 2007) are lower (0.708740 to 0.709133, average 0.708874, average $2s = 0.00002$, $n = 28$) than those from well CK-2 (0.708898 to 0.709075, average 0.708960, average $2s = 0.00001$, $n = 25$) (Table 1; Fig. 11A, B). In XC-1, the $^{87}\text{Sr}/^{86}\text{Sr}$ ratios from the dolostones of the unit 1 range from 0.708740 to 0.708933 (average 0.708838, $n = 17$), whereas those from the unit 2 range from 0.708844 to 0.709133 (average 0.708932, $n = 11$) (Fig. 11B). As with well CK-2 (Fig. 11A), there is no correlation between the $^{87}\text{Sr}/^{86}\text{Sr}$ values and Sr content in XC-1 (Fig. 11B).

The $^{87}\text{Sr}/^{86}\text{Sr}$ -depth curves and XC-1 and CK-2, are different (Fig. 12). In general, the $^{87}\text{Sr}/^{86}\text{Sr}$ ratios in XC-1 (average 0.708874) are ~ 0.00008 lower than those from CK-2 (average 0.708960). Nevertheless, as in CK-2, the $^{87}\text{Sr}/^{86}\text{Sr}$ ratios in XC-1, with the exception of a few

samples, increase from the base to the top of the formation (Fig. 12). In addition, the $^{87}\text{Sr}/^{86}\text{Sr}$ ratios of the dolostones from unit 1 in XC-1 are similar to those from the limestone in the underlying Meishan Formation in CK-2 (Fig. 12).

6. Sr source

Dating dolomitization by using the $^{87}\text{Sr}/^{86}\text{Sr}$ geochronometer is only viable if the (1) dolomitization was mediated by seawater, (2) $^{87}\text{Sr}/^{86}\text{Sr}$ values of the seawater were not modified before dolomitization took place (Fouke et al., 1996; Machel, 2000), and/or (3) dolostones did not undergo any subsequent recrystallization (Jones and Luth, 2003). As in any setting, the seawater $^{87}\text{Sr}/^{86}\text{Sr}$ values can be modified by the reaction with the limestone precursor, the overlying and underlying limestones and dolostones, older volcanic rocks, volcanoclastic or siliciclastic sediments, and/or siliceous atmospheric dust (Fouke et al., 1996; Gill et al., 1995; Jones and Luth, 2003; Machel, 2000; Zhao and Jones, 2012a). For the dolostones from well CK-2 there is no obvious correlation between the Sr content and the $^{87}\text{Sr}/^{86}\text{Sr}$ ratios (Fig. 11A). Vahrenkamp et al. (1988) suggested that relative uniform $^{87}\text{Sr}/^{86}\text{Sr}$ ratios throughout a thick dolostone succession are probably inherited from the dolomitizing fluids rather than the precursor limestones. In addition, there is no evidence that the dolomitization fluids for the massive dolostones in the Huangliu Formation were derived from the overlying or underlying formations that are formed of limestones or dolomitic limestones (Fig. 3). Although the basement of the Xisha Platform is formed of volcanic rocks and associated volcanoclastic sediments (Fig. 2A), the dolostones in the Huangliu Formation are separated from them by

limestone sequences that are up to 350 m thick. Similarly, there is no evidence of any siliciclastic sediments near Xisha Islands that could have provided any of the Sr. Although it is possible that siliceous atmospheric dust could have been carried into the area by East Asian winter monsoons, there is no obvious terra rossa in the succession on the Xisha Islands. Thus, it appears that the Sr and the $^{87}\text{Sr}/^{86}\text{Sr}$ ratio were inherited from the seawater.

That the Sr and the $^{87}\text{Sr}/^{86}\text{Sr}$ ratios in the dolostones in the Huangliu Formation were inherited from seawater is supported by the following characteristics.

- The Sr content of the dolostones in CK-2 (88 to 417 ppm, average 233 ppm) and XC-1 (139 to 205 ppm, average 176 ppm) lie within the range of Sr values (70 to 250 ppm) found in most island dolostones (Vahrenkamp and Swart, 1990; Malone et al., 1996; Budd, 1997; Jones and Luth, 2003; Swart and Melim, 2000), which has generally been considered indicative of dolomitization that was mediated by (near)-normal marine waters.
- The REE distribution patterns in the dolostones from CK-2 are similar to the REE distribution patterns of modern seawater in the South China Sea (Fig. 13).
- The lack of correlation between $\delta^{13}\text{C}$ and $\delta^{18}\text{O}$ from wells CK-2, XC-1, and XK-1 (Fig. 9B) suggests that meteoric water was not involved in the dolomitization (Budd, 1997; Warren, 2000; Swart, 2015).

The possibility that recrystallization may have reset the $^{87}\text{Sr}/^{86}\text{Sr}$ geochronometer in the dolostones of the Huangliu Formation must be considered in any assessment of the $^{87}\text{Sr}/^{86}\text{Sr}$ ratios (Jones and Luth, 2003; Ren and Jones, 2018). Mazzullo (1992) suggested that recrystallized dolomites, relative to the original dolomites, (1) are more stoichiometric, (2) have

enlarged crystals, (3) have significantly different geochemical signatures (e.g., ^{18}O , Sr content), and/or (4) display homogeneous CL signatures. The fabric-retentive fabrics of the dolostones in units 2, 3, and 4 of the Huangluei Formation in CK-2, which are similar to replacive dolostones described from other islands (Budd, 1997; Jones and Luth, 2003; Zhao and Jones, 2012b; Ren and Jones, 2017, 2018), display no evidence of recrystallization. Although the dolostones in unit 1 of the Huangluei Formation in CK-2 have fabric-destructive textures, enlarged crystals, and slightly negative $\delta^{18}\text{O}$, available data are inconsistent with the notion of recrystallization because: (1) the Ca-rich dolostones in the unit 1 (average %Ca of 55.3%) are like those in units 2, 3, and 4 with average %Ca of 55.2, 55.7, and 56.2% respectively (Fig. 8), (2) there is no obvious difference in the Sr content of unit 1 (average 198 ppm) relative to units 2, 3, and 4 (average 299, 236 and 137 ppm, respectively), (3) the zoned crystals, evident under CL, indicate that the dolomites had not been significantly recrystallized (Fig. 7). In addition, there is no evidence of dolomite recrystallization in other wells from Xisha islands (Wei et al., 2007; Zhao, 2010; Wang et al., 2015; Wang et al. 2018).

Available evidence indicates that the Sr content and the $^{87}\text{Sr}/^{86}\text{Sr}$ ratios in the dolostones of the Huangluei Formation of Xisha Island have not been modified by recrystallization. Accordingly, the $^{87}\text{Sr}/^{86}\text{Sr}$ ratios in the dolostones are thought to reflect the age of the seawater that mediated the dolomitization.

7. Timing of dolomitization

Dolomitization on most carbonate islands (e.g., Grand Cayman, Cayman Brac, Kita-daito-jima, Little Bahama Bank) appears to have taken place between the late Miocene and early Pleistocene (Table 2) (Budd, 1997; Ren and Jones, 2018). There is, however, evidence of middle Miocene dolomitization on some islands, including Curacao (Fouke et al., 1996) and late Pleistocene dolomitization on other islands such as San Salvador and Niue (Aharon et al., 1987; Vahrenkamp et al., 1991). In many cases, dolomitization has been linked to time-restricted “dolomitization events” that may have operated globally (Jones et al., 1984; Pleydell et al., 1990; Budd, 1997; Machel, 2000; Jones and Luth, 2002, 2003; MacNeil and Jones, 2003; Zhao and Jones, 2012a, b; Ren and Jones, 2017). Use of this “event-based” model has led to the notion that different islands were affected by anywhere from one to five ‘dolomitization events’, as follows:

- Kita-daito-jima – two phases of dolomitization (Ohde and Elderfield, 1992; Suzuki et al., 2006).
- Grand Cayman – two phases of dolomitization (Jones and Luth, 2003; Ren and Jones, 2017).
- Little Bahama Bank – three phases of dolomitization (Vahrenkamp et al., 1991).
- Funafuti – one or two dolomitization phases (Ohde et al., 2002)
- New Providence – two phases of dolomitization (Vahrenkamp et al., 1991).
- San Salvador – four or five phases of dolomitization (Vahrenkamp et al., 1991).

The idea of multiple dolomitization events has arisen largely from dating those events based on the $^{87}\text{Sr}/^{86}\text{Sr}$ derived from the dolostones. There are, however, problems with such an approach with much of the dating depending on the manner in which the $^{87}\text{Sr}/^{86}\text{Sr}$ ratios are interpreted. For well CK-2 on the Xisha Islands, the $^{87}\text{Sr}/^{86}\text{Sr}$ ratios range from 0.708898 at the bottom to 0.709075 at the top of the Huangliu Formation. Based on the $^{87}\text{Sr}/^{86}\text{Sr}$ -age relationship developed by MacArthur et al. (2012), this suggests that dolomitization took place between ~9.4 to 2.3 Ma. Interpretation of a histogram for the $^{87}\text{Sr}/^{86}\text{Sr}$ ratios from the dolostones in CK-2 depends largely on the class-interval that is used to segregate the values into different groups that may reflect different the different dolomitization events. A class interval of 0.00005, for example, indicates one phase of dolomitization (from ca. 9.4 to 2.3 Ma), whereas a class interval of 0.00003 suggests two phases of dolomitization (ca. 9.4 to 6 Ma and ca. 5.2 to 2.3 Ma). This problem is compounded by the fact that the error margins associated with the $^{87}\text{Sr}/^{86}\text{Sr}$ ratios translate in potential time errors of ± 0.5 to 2 Myrs (e.g., Jones and Luth, 2003; MacArthur et al., 2012), which means that the use of class intervals as low as 0.00003 is questionable.

In well CK-2, the $^{87}\text{Sr}/^{86}\text{Sr}$ ratios of the dolostones increase gradually from the bottom to the top of the Huangliu Formation, apart from a small offset in the trend in the basal part of unit 3 (Fig. 12). It appears, therefore that dolomitization became progressively younger from the base to the top of the formation. Although the $^{87}\text{Sr}/^{86}\text{Sr}$ ratios from the dolostones in well XC-1 are generally ~0.00008 lower than those in well CK-2 (Fig. 12; Table 1), the progressive increase from the bottom to the top of the Huangliu Formation is still evident. The differences between the two wells may be due to the following reasons.

- Analytical differences caused by the $^{87}\text{Sr}/^{86}\text{Sr}$ analyses being done in different laboratories. Careful checking of the analytical methods and data, however, did not reveal any obvious problems with the data from the different laboratories.
- That dolomitization in well XC-1 (~1 km from CK-2) is older than that in well CK-2.
- Geographic variations in the $^{87}\text{Sr}/^{86}\text{Sr}$ ratios of the dolomitization fluid due to modification of those fluids along their flow path. This would be akin to the geographical variations seen in other geochemical signatures of dolostones elsewhere in the world (e.g., Ren and Jones, 2017, 2018).

A similar upward-increase in the $^{87}\text{Sr}/^{86}\text{Sr}$ ratios in dolostones is also evident on many other islands throughout the world (Fig. 14), including Kita-daito-jima, Little Bahama Bank, Grand Cayman, Funafuti, New Providence, and San Salvador (Fig. 14). This pattern is evident even though the thicknesses of the dolostone successions varies from island to island (Fig. 14).

The $^{87}\text{Sr}/^{86}\text{Sr}$ data from the dolostones in well CK-2 can be attributed to (1) a series of time-synchronous events that took place at various times during the evolution of the succession, or (2) a time-transgressive process that was associated with a steady, progressive rise in sea-level. Given the problems with the interpretation of the $^{87}\text{Sr}/^{86}\text{Sr}$ data, however, it is difficult to distinguish between the two options. For the succession in CK-2 on the Xisha Islands, the ~9.4 to 2.3 Ma time-frame for dolomitization would include dolomitization events B, C, D, and E as suggested by Budd (1997). The same is also true for the dolostone successions on Grand Cayman, Little Bahama Bank, and Kita-daito-jima.

8. Discussion

8.1 Stratigraphic framework for dolomitization in Xisha Islands

The Xisha Platform is surrounded by several depressions/basins (Fig. 1B) with ocean waters > 1000 m deep (Wu et al., 2014). The oceanic isolation of the platform means that the sedimentary bedrock succession is formed entirely of carbonates because no river-borne detrital sediments have ever reached them. The presence of open marine organisms, including corals, algae, foraminifera, gastropods, and bivalves coupled the lack of evaporates or other intertidal deposits throughout the Huangliu Formation in well CK-2, clearly indicates that the original limestones all formed in shallow marine environments that were probably less than 30 m deep. This also implies that the rise in sea-level or rate of subsidence kept pace with the rate of sediment accumulation so that the water depth remained relatively constant throughout the time of active deposition. Today, the upper and basal boundaries of Huangliu Formation in well CK-2 are located 308.5 and 519 m below sea-level respectively (Fig. 4B). This depth range would only be possible if, following deposition, the formation became buried due to subsidence and/or a rise in sea-level. Irrespective of the contrasts between the sea-level curves of Vail and Mitchum (1979), Haq et al. (1987), and Miller et al. (2005) (Fig. 15), none of them show a sea-level rise of 308.5 m during post-Miocene times. Thus, available evidence suggests that the Huangliu Formation must have experienced substantial subsidence after its deposition. Wu et al. (2014) and Ma et al. (2011) also suggested that the Xisha Platform had experienced significant subsidence since the early Miocene.

The age of the Huangliu Formation in well CK-2 is difficult to establish accurately because it lacks age-diagnostic fossils. Only the maximum and minimum ages can be obtained from the underlying limestones of the Meishan Formation and the overlying limestone-dolostone succession of the Yinggehai Formation (Fig. 15). The $^{87}\text{Sr}/^{86}\text{Sr}$ ratios from the limestones at the top of the Meishan Formation (526 and 531 m) translate into ages of 12.5 ± 0.5 Ma and 12.9 ± 0.5 Ma respectively (Fig. 15), if the McArthur et al. (2012) age curves are used. In well CK-2, *Globorotalia tumida tumida* and *Globorotalia margaritae* first appear in the basal part of the Yinggehai Formation at a depth of 306 m (Fig. 15). According to Blow (1979) and Bolli and Saunders (1985), these foraminifera belong to the N18 biozone with an age of 5.0 ± 0.5 Ma. Together, this means that the Huangliu Formation is between 12.5 and 5.0 Ma old (Fig. 15). This age range is consistent with Zhao (2010) and Shao et al. (2017a) who suggested that the Huangliu Formation in wells XK-1 and XC-1 were late Miocene in age.

The ages of the internal unconformities A, B, and C cannot be established given the lack of biozone fossils and the fact that the $^{87}\text{Sr}/^{86}\text{Sr}$ ratios probably represent the time of dolomitization rather than the age of the original limestones.

8.2. Dolomitization fluids and models

The $\delta^{13}\text{C}$ and $\delta^{18}\text{O}$ values of the dolostones in the Huangliu Formation (Fig. 9A) in well CK-2 are similar to those obtained from island dolostones elsewhere in the world. The $\delta^{13}\text{C}$ values (1.0 to 3.0‰) from the Huangliu Formation, which overlap with the 0.5 to 3.2‰ range found worldwide (e.g., Budd, 1997; Ren and Jones, 2018), were probably inherited largely from

the precursor sediments or rocks. The $\delta^{18}\text{O}$ values of island dolostones have generally been linked to the temperature and/or isotopic composition of the dolomitizing fluids (Budd, 1997; Zhao and Jones, 2012a; Swart, 2015; Ren and Jones, 2017). For the Huangliu Formation in well CK-2, the $\delta^{18}\text{O}$ values, which range from 2.0 to 4.7‰, are similar to the $\delta^{18}\text{O}$ values (0.5 to 4.5‰) derived from most island dolostones (e.g., Budd, 1997; Ren and Jones, 2018). The lack of evaporitic minerals in the Huangliu Formation suggests that hypersaline brines were not involved in the dolomitization process. The lack of correlation between the $\delta^{13}\text{C}$ and $\delta^{18}\text{O}$ values also suggests that the dolomitization fluids were not mixed seawater and freshwater (cf., Budd, 1997; Warren, 2000; Swart, 2015).

Budd (1997) suggested that normal or slightly modified seawater probably mediated the development of most island dolostones. This notion is supported by the recent study of the dolostones on Grand Cayman and Cayman Brac (Zhao and Jones, 2012a, b; Ren and Jones, 2017). The same situation appears to be true for the dolostones in well CK-2. As suggested by Wang et al. (2018), the dolomitization fluids in well XK-1 (or ZK-1) were dominated by slightly evaporated seawater. Further distinction between normal seawater and slightly evaporated seawater based on $\delta^{18}\text{O}$ alone is virtually impossible due to the uncertainties in $\delta^{18}\text{O}$ interpretations (Budd, 1997).

Ren and Jones (2017, 2018), based on a detailed study of island dolostones on Grand Cayman, argued that geographic variations in the attributes of island dolostones are critical aspects of any dolomitization model developed to explain their origin. For the Cayman Formation on Grand Cayman, they divided the dolostones geographically into the peripheral

dolostone, transitional dolostone, and the interior limestone and dolostone zones based on the systematic changes in the percentages of LCD and HCD, the %Ca, and the C/O isotopes of the dolostones from the coastline to the interior of the island. It is difficult to apply this model directly to the dolostones in the Huangliu Formation on the Xisha Islands because detailed information is available only from well CK-2 and it is therefore impossible to map geographical variations. For the dolostones in well CK-2, the %LCD (average 28%), the %Ca (average 55.4%), the $\delta^{13}\text{C}$ values (average 2.3‰), and the $\delta^{18}\text{O}$ values (average 3.3‰) are similar to those considered characteristic of the “transition zone” on Grand Cayman.

8.3. Time-transgressive dolomitization process

The time frame (~9.4 to 2.3 Ma) during which dolomitization of the limestones that belonged to the Huangliu Formation in well CK-2 took place is similar to that on many other islands, including Grand Cayman, Cayman Brac, Kita-daito-jima, and the Little Bahama Bank (Table 2). It is for this reason that dolomitization has commonly been linked to global factors (Budd, 1997; Jones and Luth, 2003; Ren and Jones, 2018). During this period, significant climatic changes and large fluctuations in sea-level were driven by glaciations in the southern and northern hemispheres (e.g., Lear et al., 2000; Zachos et al., 2001). Thus, eustatic changes in sea-level have been implicated in the global dolomitization events (Budd, 1997; Jones and Luth, 2003; Suzuki et al., 2006; Zhao and Jones, 2012a). The thicknesses of the dolostone successions varies from island to island (Fig. 14), suggesting that global sea-level changes may not have been the only factor involved. The dolostone in the Huangliu Formation on Xisha Islands, for example,

attain a maximum thickness of 260 m in XY-1 (Fig. 4A), which is almost twice as thick as the dolostones found in the Cayman Formation on Grand Cayman (Ren and Jones, 2017). Between ~9.4 and 2.3 Ma, which is the time frame during which most dolomitization seems to have occurred, sea-level change was generally < 150 m according to the sea-level curves developed by Haq et al. (1987), Vail and Mitchum (1979), and Miller et al. (2005) (Fig. 15). Given the variance between the sea-level curves proposed by these authors, the 150 m can probably be considered as the absolute maximum change. Even so, the 260 m-thickness of the dolostones in the Huangliu Formation is far in excess of the sea-level change. It appears, therefore, that subsidence must have also played a significant role in the developed of the dolostone successions on the Xisha Platform.

Wu et al. (2014), based on a detailed study of the area, demonstrated that the Huaguang Depression, Changchang Depression, and Zhongjian Basin found around the Xisha Platform (Fig. 1B) have been actively subsiding over the last 50 Ma. Such subsidence probably accounts for the thickness of the shallow-water deposits that form the Huangliu Formation. Likewise, rapid tectonic subsidence during the late Miocene (from 10.5 to 5.5 Ma), as proposed by Wu et al. (2014), may also explain the transgressive pattern evident from the $^{87}\text{Sr}/^{86}\text{Sr}$ ratios (Fig. 12). It is also probable that the situation was further complicated by eustatic changes in sea-level that took place at the same time as the subsidence. The unconformities found within the Huangliu Formation probably formed in response to the combined effects of the subsidence and eustatic sea level changes. As yet, however, it is impossible to separate the effects of subsidence from the effects of the eustatic sea level changes.

Globally, the variable thicknesses of the dolostone successions on different islands may reflect differences in local tectonic subsidence (Fig. 16). Thus, islands that have the thickest dolostone successions that formed between ~10 and 1 Ma, are those that experienced high subsidence rates (Fig. 16). The dolostone succession in the Huangliu Formation on Xisha Islands, for example, is up to 260 m thick (Zhao, 2010; Wang et al., 2015), whereas on islands such as Grand Cayman and Kita-daito-jima that experienced minimal subsidence or uplift the dolostone successions are significantly thinner (Fig. 16).

Evidence from the dolostones in the Huangliu Formation found in well CK-2 suggests that dolomitization may have been a continuous time-transgressive process. There is no clear evidence of more than one phase of replacive dolomitization. Even the contrast between the fabric-destructive textures in unit 1 and the fabric-retentive textures in units 2, 3, and 4 (Fig. 4B) cannot be considered as unequivocal evidence of multiple phases of dolomitization given that these contrasting fabrics have also been attributed other factors such as mineral composition and fabric of the precursor limestone and/or the temperature and composition of the dolomitizing fluids (Sibley, 1987; Sibley et al., 1993; Warren, 2000; Machel, 2004). On other islands, including Grand Cayman, such dolostone fabrics are geographically variable (e.g., Ren and Jones, 2018).

The time-transgressive dolomitization proposed for the Huangliu Formation may have been controlled by subsidence and/or global sea-level changes. Delineating the contributions of each of these processes, however, is difficult. The tectonic development of the Xisha Platform, which is based largely on seismic data (Wu et al., 2014) is not well known in terms of subsidence rates.

Similarly, various sea-level curves such as those proposed by Haq et al. (1987), Vail and Mitchum (1979), and Miller et al. (2005) are characterized by significant differences in terms of the timing and magnitude of sea level changes during the time when dolomitization took place on the Xisha Platform (Fig. 15). Although subsidence must have controlled, at least in part, the time-transgressive dolomitization on these islands, it is impossible to clearly delineate its impact relative to the impact of eustatic changes in sea level.

9. Conclusions

Detailed analysis of the dolostone succession in the Late Miocene, unconformity-bounded Huangliu Formation in well CK-2 on Xisha Islands, located in the South China Sea, has led to the following important conclusions.

- The Huangliu Formation comprises four units (in ascending order, 1, 2, 3, and 4) that are separate from each other by unconformities. Unit 1 is formed of tan, well-indurated medium to coarsely crystalline, fabric-destructive dolostones, whereas units 2, 3, and 4 are composed of grey, fine to medium crystalline fabric-retentive dolostones.
- Available evidence indicates that dolomitization was probably mediated by normal or slightly modified seawater.
- Dolomitization took place between ~9.4 to 2.3 Ma during a (semi-)continuous time-transgressive dolomitization process.
- The transgressive phase in sea-level that promoted dolomitization of the Huangliu Formation was controlled by local tectonic subsidence and global eustatic changes in sea-level. The

relative importance of subsidence and sea-level changes in this process are, however, difficult to establish because of the lack of precise tectonic data and the conflicting views regarding sea-level oscillations during the time when dolomitization was taking place.

Acknowledgements

This work was funded by the National Natural Science Foundation of China (No. 91428203), Science and Technology Project of Guangxi (Nos. AD17129063 and AA17204074), BaGui Fellowship from Guangxi Province, Guangxi Natural Science project (No.2014BGXZGX03) and Guangxi Youth Science Fund Project (2017GXNSFBA198242). We are grateful to the drilling crews from the Guizhou Bureau of Geology and Mineral Resources, who spent long days drilling the wells; numerous staff members from the South China Sea Institute of Oceanology and Wuhan Institute of Rock and Soil Mechanics, Chinese Academy of Sciences, who helped to collect samples during drilling; Xinfu Zhao, who helped take the cathodoluminescent photomicrographs; Yanrong Liu, who ran the EMPA analyses; and Shaopeng Wang, who helped take carbon and oxygen isotope data.

References

- Aharon, P., Socki, R.A., Chan, L., 1987. Dolomitization of atolls by sea water convection flow: test of a hypothesis at Niue, South Pacific. *J. Geol.* 95, 187-203.
- Aissaoui, D.M., Buigues, D., Purser, B.H., 1986. Model of reef diagenesis: Mururoa Atoll, French Polynesia, In: Schroeder, J.H., Purser, B.H. (Eds.), *Reef Diagenesis*. Springer, Berlin, pp. 27-52.
- Alibo, D.S., Nozaki, Y., 2000. Dissolved rare earth elements in the South China Sea: geochemical characterization of the water masses. *J. Geophys. Res.: Oceans.* 105, 28771-28783.
- Blow, W.H., 1979. The Cainozoic Globigerinida: A Study of the Morphology, Taxonomy, Evolutionary Relationships and the Stratigraphical Distribution of some Globigerinida (mainly Globigerinacea). E.J. Brill, Leiden.
- Bolli, H.M., Saunders, J.B., 1985. Oligocene to Holocene low latitude planktonic foraminifera. In: Bolli, H.M., Saunders, J.B., Perch-Nielsen, K. (Eds.), *Plankton Stratigraphy*. Cambridge Univ. Press, Cambridge, pp. 155-262.
- Budd, D.A., 1997. Cenozoic dolomites of carbonate islands: their attributes and origin. *Earth Sci. Rev.* 42, 1-47.
- Dawans, J.M., Swart, P.K., 1988. Textural and geochemical alternations in Late Cenozoic Bahamian dolomites. *Sedimentology* 35, 385-403.
- Fouke, B.W., Beets, C.J., Meyers, W.J., Hanson, G.N., Melillo, A.J., 1996. $^{87}\text{Sr}/^{86}\text{Sr}$ chronostratigraphy and dolomitization history of the Seroe Domi Formation, Curaçao (Netherlands Antilles). *Facies* 35, 293-320.
- Gill, I.P., Moore, C.H., Aharon, P., 1995. Evaporitic mixed-water dolomitization on St. Croix, U.S.V.I. *J. Sediment. Res.* 65, 591-604.
- Haq, B.U., Hardenbol, J., Vail, P.R., 1987. Chronology of fluctuating sea levels since the Triassic. *Science* 235, 1156-1167.
- Jones, B., 2007. Inside-Out Dolomite. *J. Sediment. Res.* 77, 539-551.
- Jones, B., Lockhart, E.B., Squair, C., 1984. Phreatic and vadose cements in the Tertiary Bluff Formation of Grand Cayman Island, British West Indies. *Bull. Can. Pet. Geol.* 32, 382-397.

- Jones, B., Luth, R.W., 2002. Dolostones from Grand Cayman, British West Indies. *J. Sediment. Res.* 72, 559-569.
- Jones, B., Luth, R.W., 2003. Temporal evolution of Tertiary dolostones on Grand Cayman as determined by $^{87}\text{Sr}/^{86}\text{Sr}$. *J. Sediment. Res.* 73, 187-205.
- Jones, B., Luth, R.W., Macneil, A.J., 2001. Powder X-Ray diffraction analysis of homogeneous and heterogeneous sedimentary dolostones. *J. Sediment. Res.* 71, 790-799.
- Kuang, Z., Guo, Y., Wang, L., Liang, J., Sha, Z., 2014. Evolution of the Late Miocene atoll systems offshore Xisha Islands. *Sci. China: Earth Sci.* 57, 3084-3096.
- Lear, C.H., Elderfield, H., Wilson, P.A., 2000. Cenozoic deep-sea temperatures and global ice volumes from Mg/Ca in benthic foraminiferal calcite. *Science* 287, 269-272.
- Ma, Y., Wu, S., Lv, F., Dong, D., Sun, Q., Lu, Y., Gu, M., 2011. Seismic characteristics and development of the Xisha carbonate platforms, northern margin of the South China Sea. *J. Asian Earth Sci.* 40, 770-783.
- Machel, H.G., 2000. Dolomite formation in Caribbean Islands: driven by plate tectonics?!. *J. Sediment. Res.* 70, 977-984.
- Machel, H.G., 2004. Concepts and models of dolomitization: a critical reappraisal. In: Braithwaite, C.J.R., Rizzi, G., Darke, G (Eds), *The Geometry and Petrogenesis of Dolomite Hydrocarbon Reservoirs*. Geol. Soc. London Spec. Publ. 235, pp. 7-63.
- MacNeil, A., Jones, B., 2003. Dolomitization of the Pedro Castle Formation (Pliocene), Cayman Brac, British West Indies. *Sediment. Geol.* 162, 219-238.
- Malone, M.J., Baker, P.A., Burns, S.J., 1996. Recrystallization of dolomite: an experimental study from 50-200°C. *Geochim. Cosmochim. Acta.* 60, 2189-2207.
- Mazzullo, S.J., 1992. Geochemical and neomorphic alteration of dolomite: a review. *Carbonates Evaporites.* 7, 21-37.
- Mcarthur, J.M., Howarth, R.J., Bailey, T.R., 2001. Strontium isotope stratigraphy: LOWESS Version 3: best fit to the marine Sr-isotope curve for 0-509 Ma and accompanying look-up table for deriving numerical age. *J. Geol.* 109, 155-170.

- McArthur, J.M., Howarth, R.J., Shields, G.A., 2012. Strontium isotope stratigraphy. In: Gradstein, F.M. (Ed.), *The Geologic Time Scale*. Elsevier Science Limited, pp. 127-144.
- Mckenzie, J.A., Hodell, D.A., Mueller, P.A., Mueller, D.W., 1988. Application of strontium isotopes to late Miocene-early Pliocene stratigraphy. *Geology* 16, 1022-1025.
- Meyers, W.J., Lu, F.H., Zachariah, J.K., 1997. Dolomitization by mixed evaporite brines and freshwater, Upper Miocene carbonates, Nijar, Spain. *J. Sediment. Res.* 67, 898-912.
- Miller, K.G., Komins, M.A., Browning, J.V., Wright, J.D., Mountain, G.S., Katz, M.E., Sugarman, P.J., Cramer, B.S., Christie-Blick, N., Pekar, S.F., 2005. The Phanerozoic record of global sea-level change. *Science* 310, 1293-1298.
- Ng, K.C., 1990. Diagenesis of the Oligocene–Miocene Bluff Formation of the Cayman Islands — a petrographic and hydrogeochemical approach. Ph.D. thesis. University of Alberta, Edmonton (344 pp).
- Ohde, S., Elderfield, H., 1992. Strontium isotope stratigraphy of Kita-daito-jima Atoll, North Philippine Sea: implications for Neogene sea-level change and tectonic history. *Earth Planet. Sci. Lett.* 113, 473-486.
- Ohde, S., Greaves, M., Masuzawa, T., Buckley, H.A., Woesik, R.V., Wilson, P.A., Pirazzoli, P.A., Elderfield, H., 2002. The chronology of Funafuti Atoll: revisiting an old friend. *Proc. R. Soc. A.* 458, 2289-2306.
- Pleydell, S.M., Jones, B., Longstaffe, F.J., Baadsgaard, H., 1990. Dolomitization of the Oligocene-Miocene Bluff Formation on Grand Cayman, British West Indies. *Can. J. Earth. Sci.* 27, 1098-1110.
- Ren, M., Jones, B., 2017. Spatial variations in the stoichiometry and geochemistry of Miocene dolomite from Grand Cayman: implications for the origin of island dolostone. *Sediment. Geol.* 348, 69-93.
- Ren, M., Jones, B., 2018. Genesis of island dolostones. *Sedimentology*. [https:// doi: 10.1111/sed.12455](https://doi.org/10.1111/sed.12455).
- Saller, A.H., 1984. Petrologic and geochemical constraints on the origin of subsurface dolomite, Enewetak Atoll an example of dolomitization by normal seawater. *Geology* 12, 217-220.
- Shao, L., Li, Q., Zhu, W., Zhang, D., Qiao, P., Liu, X., You, L., Cui, Y., Dong, X., 2017a. Neogene carbonate platform development in the NW South China Sea: litho-, bio- and chemo-stratigraphic evidence. *Mar. Geol.* 385, 233-243.

- Shao, L., Cui, Y., Qiao, P., Zhang, D., Liu, X., Zhang, C., 2017b. Sea-level changes and carbonate platform evolution of the Xisha Islands (South China Sea) since the Early Miocene. *Palaeogeogr. Palaeoclimatol. Palaeoecol.* 485, 504-516.
- Sibley, D.F., Gregg, J.M., 1987. Classification of dolomite rock texture. *J. Sediment. Res.* 57, 967-975.
- Sibley, D.F., Gregg, J.M., Brown, R.G., Laudon, P.R., 1993. Dolomite crystal size distribution, In: Rezak, R., Lavoie, D.L. (Eds), *Carbonate Microfabrics*. Springer, New York, pp. 195-204.
- Suzuki, Y., Iryu, Y., Inagaki, S., Yamada, T., Aizawa, S. and Budd, D.A., 2006. Origin of atoll dolomites distinguished by geochemistry and crystal chemistry: Kita-daito-jima, northern Philippine Sea. *Sediment. Geol.* 183, 181-202.
- Swart, P.K., Melim, L.A., 2000. The origin of dolomites in Tertiary sediments from the margin of Great Bahama Bank. *J. Sediment. Res.* 70, 738-748.
- Swart, P.K., 2015. The geochemistry of carbonate diagenesis: the past, present and future. *Sedimentology* 62, 1233-1304.
- Taylor, S.R., McLennan, S.M., 1985. *The continental crust: its composition and evolution*. Blackwell Sci., Oxford, pp. 311-313.
- Vahrenkamp, V.C., Swart, P.K., Ruiz, J., 1988. Constraints and interpretation of $^{87}\text{Sr}/^{86}\text{Sr}$ ratios in Cenozoic dolomites. *Geophys. Res. Lett.* 15, 385-388.
- Vahrenkamp, V.C., Swart, P.K., 1990. New distribution coefficient for the incorporation of strontium into dolomite and its implications for the formation of ancient dolomites. *Geology* 18, 387-391.
- Vahrenkamp, V.C., Swart, P.K., Ruiz, J., 1991. Episodic dolomitization of Late Cenozoic carbonates in the Bahamas - evidence from strontium isotopes. *J. Sediment. Petrol.* 61, 1002-1014.
- Vahrenkamp, V.C., Swart, P.K., 1994. Late Cenozoic dolomites of the Bahamas: metastable analogues for the genesis of ancient platform dolomites, In: Purser, B.H., Tucker, M.E., and Zenger, D.L. (Eds.), *Dolomites: A Volume in Honour of Dolomieu*. Int. Assoc. Sedimentol. Spec. Publ., pp.133-153.
- Vail, P.R., Mitchum, R.M., 1979. Global cycles of relative changes of sea level from seismic stratigraphy: resources, comparative structure and eustatic changes in sea level, In: *Geological and Geophysical Investigations of Continental Margins*. A.A.P.G. Memoir, pp. 469-472.

- Wang, Z., Shi, Z., Zhang, D., Huang, K., You, L., Duan, X. and Li, S., 2015. Microscopic features and genesis for Miocene to Pliocene dolomite in well Xike-1, Xisha Islands. *Earth Sci. J. China Univ. Geosci.* 40, 633-644 (in Chinese with English abstract).
- Wang, Z., Huang, K., Zhang, D., You, L., Liu, X., Luo, W., 2018. Maturation of Neogene dolomite from Xuande Atoll of Xisha archipelago, the South China Sea. *Mar. Pet. Geol.* 92, 51-64.
- Wei, X., Zhu, Y.J., Xu, H., Zhao, G.C. and Li, Y.X., 2007. Discussion on Neogene dolostone forming condition in Xisha Islands: evidences from isotope C and O and fluid inclusions. *Acta Petrol. Sin.* 22, 2394-2404 (in Chinese with English abstract).
- Wei, X. and Jia, C.Z., 2008. Dolomitization Characteristics of carbonate rock in Xisha Islands and its formation: a case study of Well Xichen-1, *J. Jilin Univ.* 38, 217-224 (in Chinese with English abstract).
- Warren, J., 2000. Dolomite: occurrence, evolution and economically important associations. *Earth Sci. Rev.* 52, 1-81.
- Wheeler, C.W., Aharon, P., Ferrell, R.E., 1999. Successions of late Cenozoic platform dolomites distinguished by texture, geochemistry, and crystal chemistry; Niue, South Pacific. *J. Sediment. Res.* 69, 239-255.
- Wu, S., Yang, Z., Wang, D., Lü, F., Lüdmann, T., Fulthorpe, C., Wang, B., 2014. Architecture, development and geological control of the Xisha carbonate platforms, northwestern South China Sea. *Mar. Geol.* 350, 71-83.
- Xiu, C., Zhang, D.J., Zhai, S.K., Liu, X.Y., Chao, J.Q., Bi, D.J., and Chen, K., 2017. REE geochemical characteristics and diagenetic environments of reef dolostone in Shi Island, Xisha Islands. *Mar. Sci. Bull.* 36, 151-159 (in Chinese with English abstract).
- Zachos, J., Pagani, M., Sloan, L., Thomas, E., Billups, K., 2001. Trends, rhythms, and aberrations in global climate 65 Ma to present. *Science* 292, 686-693.
- Zhao, H., Jones, B., 2012a. Origin of "island dolostones": a case study from the Cayman Formation (Miocene), Cayman Brac, British West Indies. *Sediment. Geol.* 243, 191-206.
- Zhao, H., Jones, B., 2012b. Genesis of fabric-destructive dolostones: a case study of the Brac Formation (Oligocene), Cayman Brac, British West Indies. *Sediment. Geol.* 267, 36-54.

Zhao, H.W., 2013. Origin of island dolostones: case study based on Tertiary dolostones from Cayman Brac, British West Indies. Ph.D. Thesis. University of Alberta, Edmonton (207 pp).

Zhao, Q., 2010. The sedimentary research about reef carbonate in Xisha Islands Waters. PhD. Thesis. Chinese Academy of Sciences, Qingdao (158 pp) (in Chinese with English abstract).

ACCEPTED MANUSCRIPT

Figure captions:

- Fig. 1.** (A) Location of Xisha Islands (Paracel Islands) (red rectangle) in South China Sea. (B) Map of Xisha Platform surrounded by various deep-water basins and depressions. Black line indicates line of cross-section shown in Figure 2. (C) Chenhang Dao showing locations of wells XC-1 and CK-2. (D) Yongxing Dao and Shi Dao showing locations of wells XY-1 and XK-1.
- Fig. 2.** (A) Cross-section through the Xisha Platform showing location of dolostones in Huangliu Formation. See Fig. 1B for the location of the cross section. (B) Schematic diagram showing faults configuration of the Xisha Platform before the early Miocene (modified from Wu et al., 2014, their Fig. 9).
- Fig. 3.** Stratigraphic succession on Xisha Platform based on the core from well CK-2 (see Fig. 1C for location) showing distribution of lithologies and depositional settings in each formation.
- Fig. 4.** (A) Stratigraphic correlation between wells XC-1, CK-2, XY-1, and XK-1 (Fig. 1B). (B) The Huangliu Formation in well CK-2 showing positions of unconformities A, B, and C that define the internal divisions of the formation. Right side of diagram summarizes main features of the dolostones in the Huangliu Formation.
- Fig. 5.** Thin section photomicrographs (plane polarized light) of dolostones from the unit 1 of the Huangliu Formation. Depths specified in upper right corner of each image are below present-day sea-level. (A) Fabric-destructive dolostone formed of coarse, subhedral to euhedral dolomite crystals. (B) Fabric-destructive dolostone formed of medium-coarse dolomite crystals and rare red algae fragments (RA). Note limpid dolomite cement lining secondary pores (P). (C) Fabric-destructive dolostone with small patches of cement (C) and scattered pores (P). (D) Euhedral dolomite crystals with hollow cores (h)

and clear rims (R). (E) Red algae (RA) fragment mimetically replaced by dolomite. (F) Dissolution molds (M) with no cements.

Fig. 6. Thin section photomicrographs (plane polarized light) of dolostones from units 2, 3, and 4 of the Huangliu Formation. Depths specified in upper right corner of each image are below present-day sea level. (A) Mimetic, finely crystalline dolostone with well-preserved foraminifera (F) and red algae (RA) held in dolomitized matrix. (B) Finely crystalline dolostone with well-preserved *Halimeda* (H) and foraminifera (F) and limpid cements (C) in pores. (C) Finely crystalline dolostone with patches of coarse dolomite cements (C). (D) Euhedral zoned dolomite with clear rims (R). Note one crystal with possible dolomite (D) in center forming inside-out dolomite, and other crystals have hollow cores (h). (E) Finely crystalline dolostone with dolomite cements (C) lining the dissolution molds (M). (F) Dissolution molds (foraminifera ?) (M). (G) Finely crystalline dolostone with crystalline matrix and dolomitized red algae fragments (RA). (H) Well-preserved *Halimeda* (H) fragments. (I) Aragonite skeleton (?) was partly replaced by dolomite.

Fig. 7. Cathodoluminescence (CL) images of dolostones from the Huangliu Formation of well CK-2. Depths in upper right corners are below present-day sea level. (A) Finely crystalline dolomites in the units 2, 3, and 4, showing relative dark luminescent and dull red CL. Matrices have dark luminescent mottled with some bright spots. Cements (C) display dull red CL with some zoning. (B) Medium-coarse crystalline dolomites in unit 1 showing bright red CL with scattered bright spots. Note the crystalline dolomites with zoning.

Fig. 8. Vertical variations in %Ca in well CK-2 showing (A) %Ca in the LCD, the average %Ca, and the %Ca in the HCD, and (B) relative percentages of LCD and HCD.

Fig. 9. Oxygen and carbon isotopes of dolomites in the Huangliu Formation. (A) Cross-plots of $\delta^{18}\text{O}$ and $\delta^{13}\text{C}$ of dolomites from the units 1, 2, 3, and 4 in well CK-2. (B) Cross-plots of $\delta^{18}\text{O}$ and $\delta^{13}\text{C}$ of dolomites from the dolostones of wells CK-2, XC-1, and XK-1. Data for wells XC-1 and XK-1 are from Zhao (2010, his Table 4.4) and Wang et al. (2015, their Fig.6), respectively.

Fig. 10. Stratigraphic variations of $\delta^{18}\text{O}$ and $\delta^{13}\text{C}$ in dolostones from wells XC-1 (A), CK-2 (B), and XK-1 (C). The $\delta^{18}\text{O}$ and $\delta^{13}\text{C}$ data of wells XC-1 and XK-1 are from Zhao (2010, his Table 4.4) and Wang et al. (2015, their Fig. 2), respectively.

Fig. 11. Bivariant graphs showing relationships between $^{87}\text{Sr}/^{86}\text{Sr}$ and Sr content of the dolostones in the Huangliu Formation in wells CK-2 (A) and XC-1 (B). The $^{87}\text{Sr}/^{86}\text{Sr}$ and Sr data for well XC-1 are from Wei et al. (2007, their Table 1).

Fig. 12. Comparison of $^{87}\text{Sr}/^{86}\text{Sr}$ -depth curves for wells CK-2 and XC-1 (shaded area indicates ± 2 sigma). The $^{87}\text{Sr}/^{86}\text{Sr}$ for seawater at Messinian-Pliocene boundary from MaKenzie et al. (1988) and Meyers et al. (1997). The $^{87}\text{Sr}/^{86}\text{Sr}$ data of well XC-1 are from Wei et al. (2007, their Table 1).

Fig. 13. The PAAS- normalized REE patterns for dolostones from the Huangliu Formation of well CK-2 and seawater from the South China Sea (Alibo and Nozaki, 2000).

Fig. 14. The $^{87}\text{Sr}/^{86}\text{Sr}$ -depth curves of different Cenozoic island dolostones (see Table 2). The $^{87}\text{Sr}/^{86}\text{Sr}$ for seawater at Messinian-Pliocene boundary from MaKenzie et al. (1988) and Meyers et al. (1997).

Fig. 15. Stratigraphic succession in well CK-2, global sea-level curves (from Haq et al., 1987, their Fig. 2; Vail and Mitchum (1979, their Fig. 3), and Miller et al. (2005, their Fig. 4)), subsidence curves for the basins and depressions around the Xisha Uplift (from Wu et al. (2014, their Fig. 10), and ages of dolomitization age of island dolostones throughout the world (based on data from Table 2).

Fig. 16. Comparison of the thicknesses of the island dolostone successions on islands in different tectonic settings.

ACCEPTED MANUSCRIPT

Fig.1

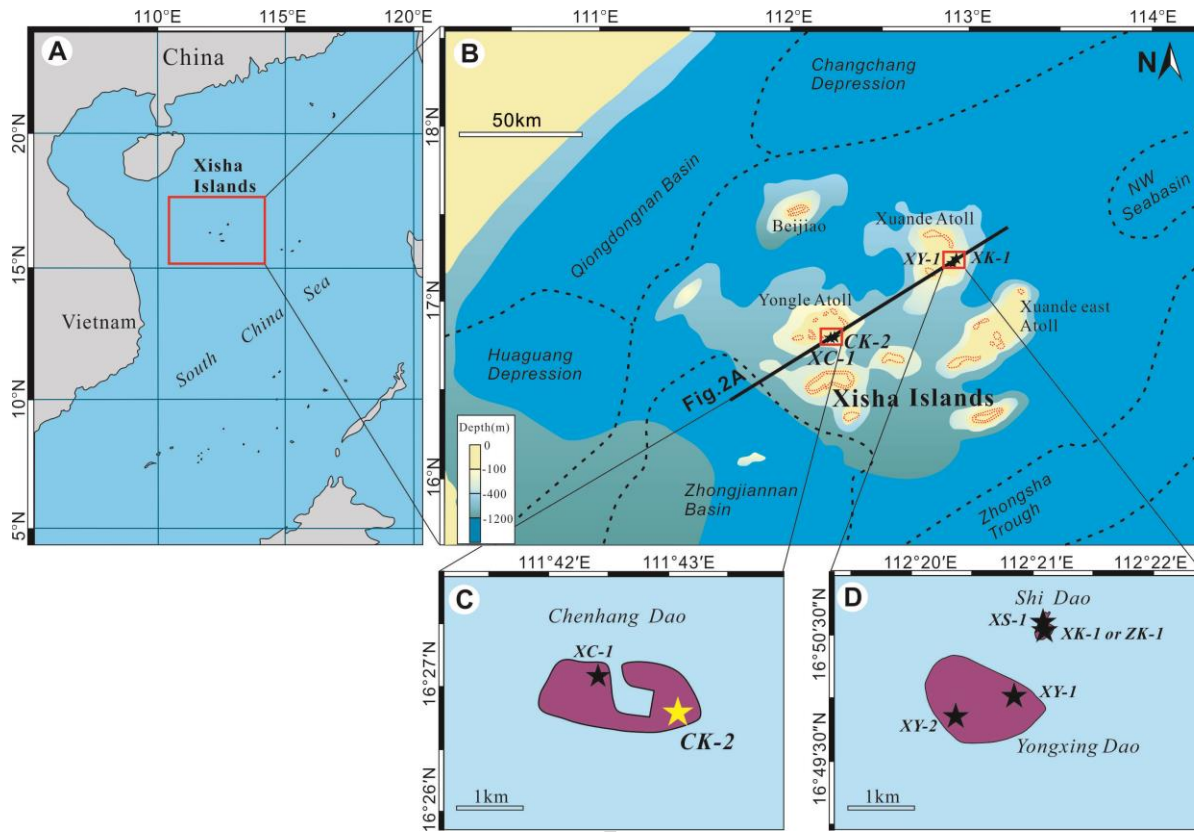


Fig. 2

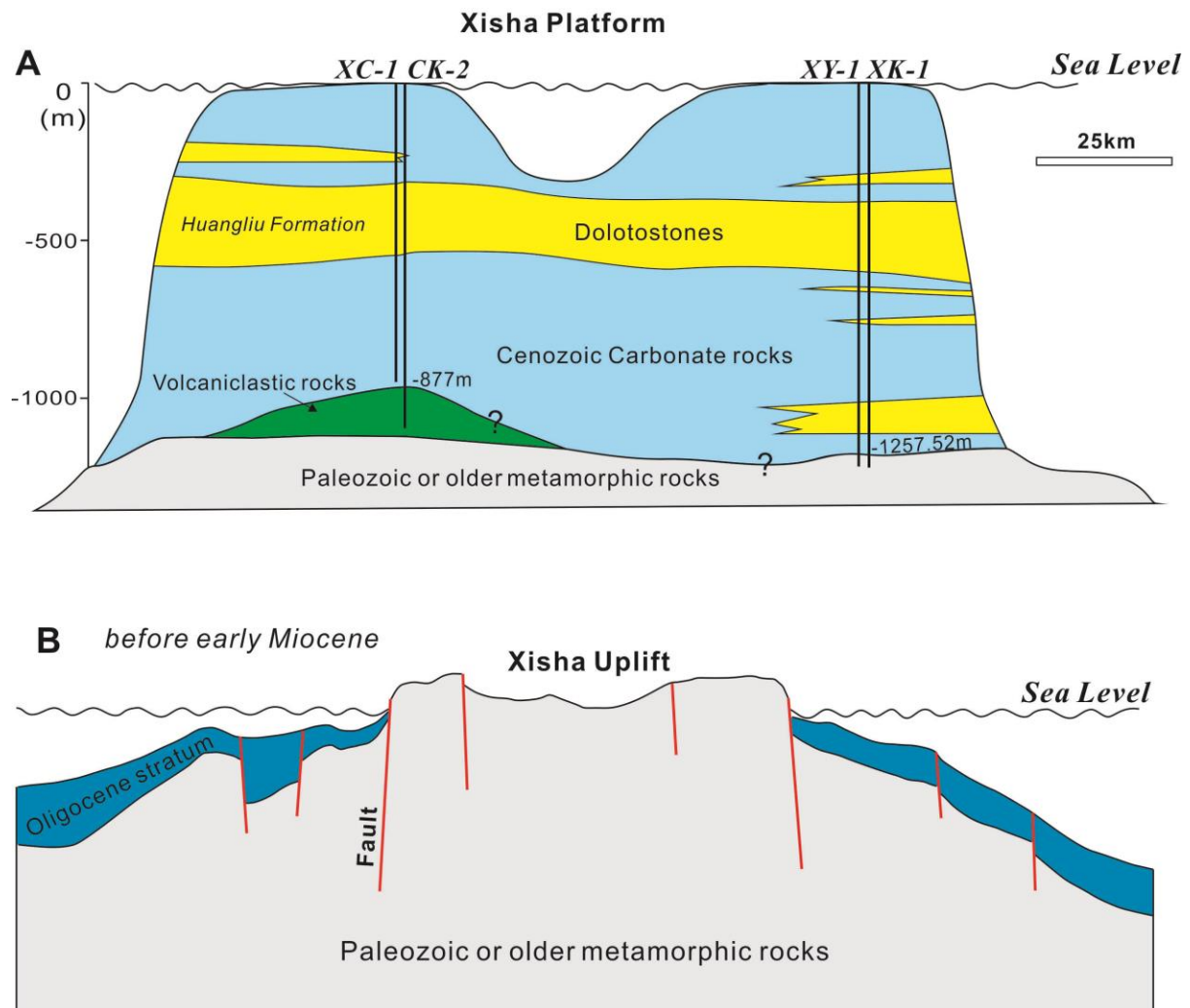


Fig. 3

AGE	FORMATION	LITHOLOGY	DEPOSITIONAL SETTINGS
HOL.		coral debris	
PLEISTOCENE	<i>Unconformity</i> Ledong Formation	Coral framestones with coralline algae bindstones	Outer-Inner reef flat
		Lagoonal sand with biologic debris	Lagoon
PLIOCENE	Yinggehai Formation	Weakly-moderately dolomitized bioclastic limestones	Inner reef flat-Lagoon
LATE MIOCENE	<i>Unconformity</i> Huangliu Formation	Dolostones (fabric-retentive)	Outer-Inner reef flat
		Dolostones (fabric-destructive)	
EALY-MIDDLE MIOCENE	<i>Unconformity</i> Meishan Formation	Lagoonal sand with coralline algae bindstones and coral rubbles	Lagoon
		<i>Unconformity</i> Sanya Formation	Lagoonal sand with foraminifera and biologic debris
		Volcanic basement	





	Limestone
	Dolostone
	Unconsolidated deposits
	Volcaniclastic rocks

Fig. 4

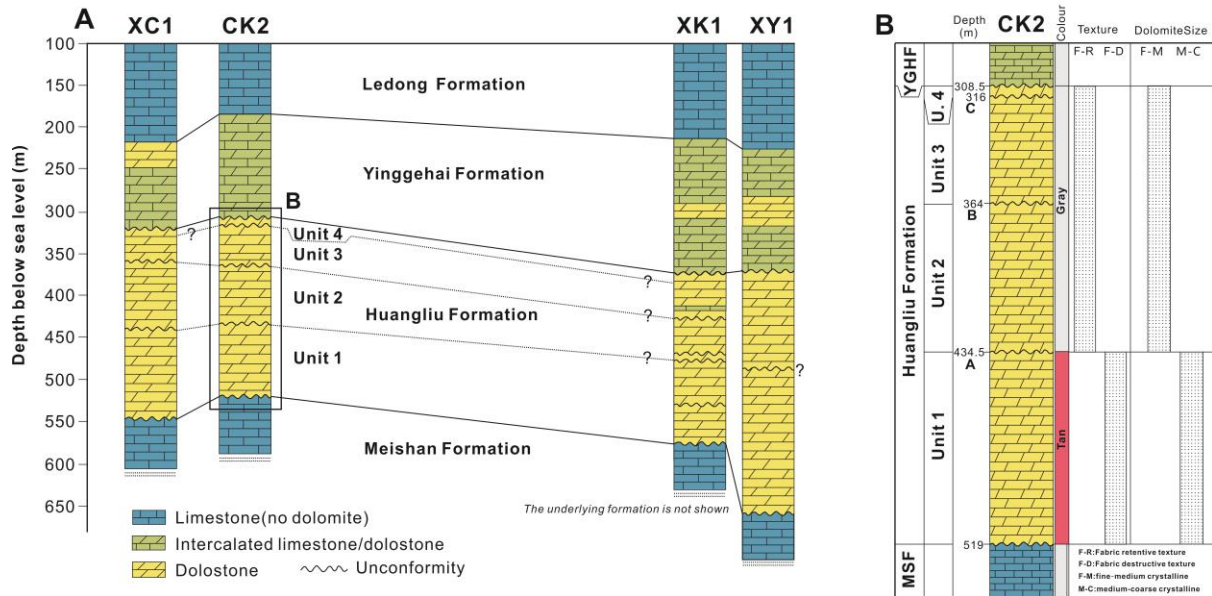


Fig. 5

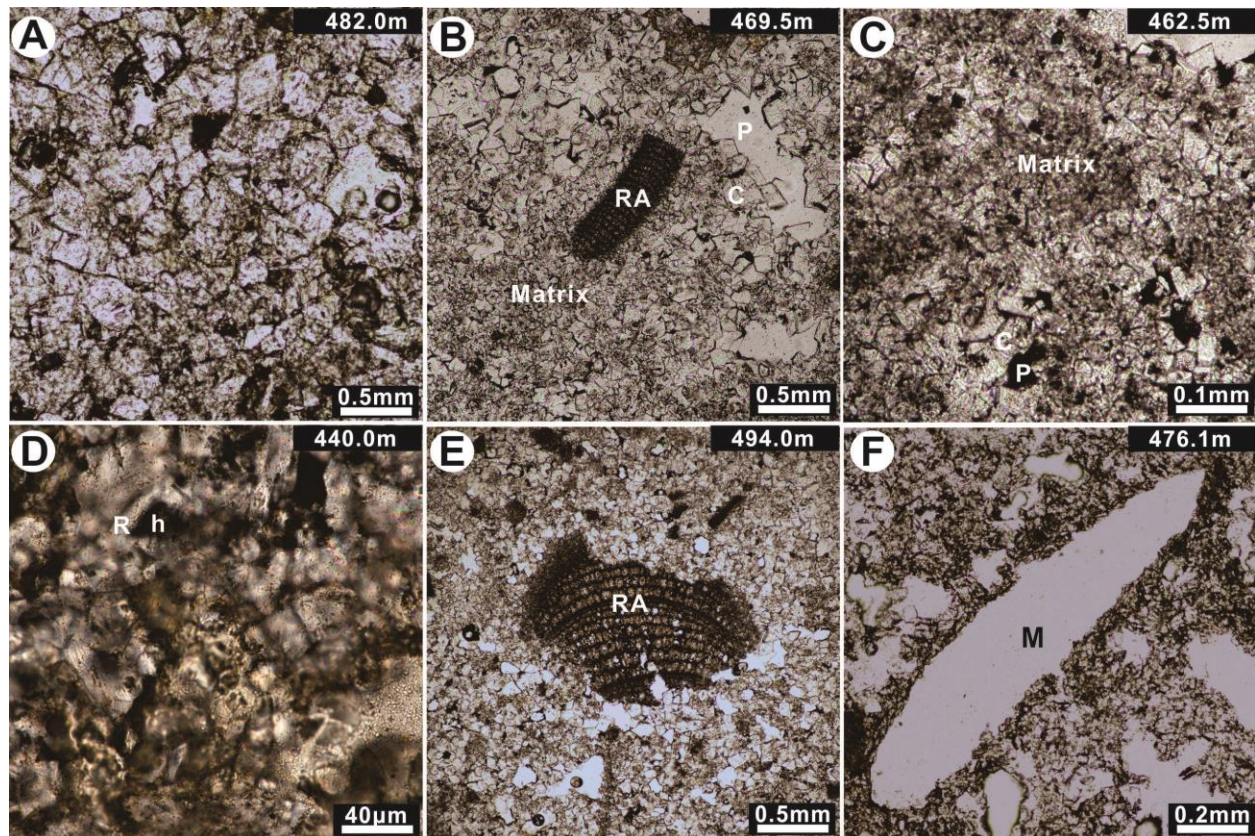


Fig. 6

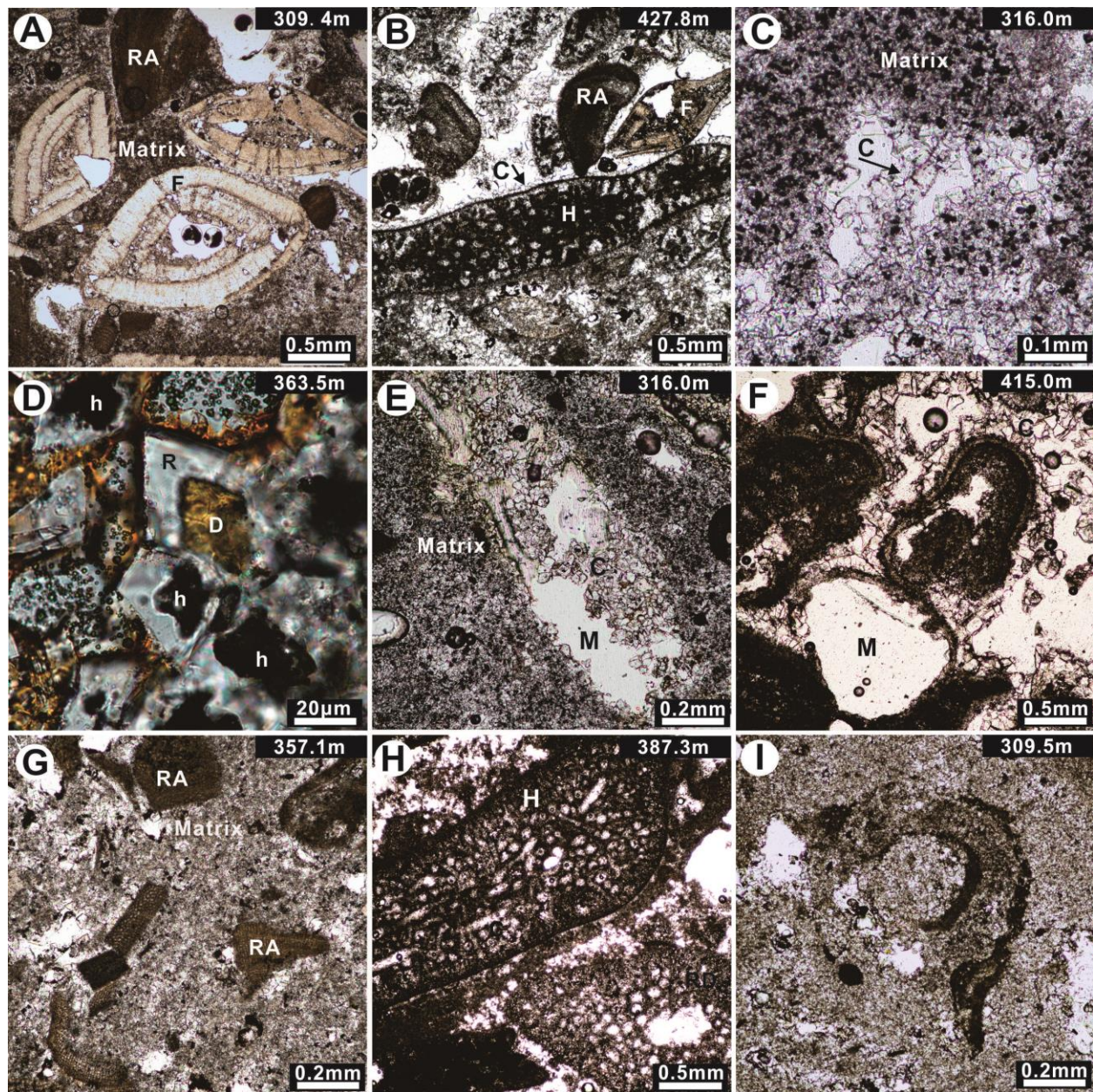


Fig. 7

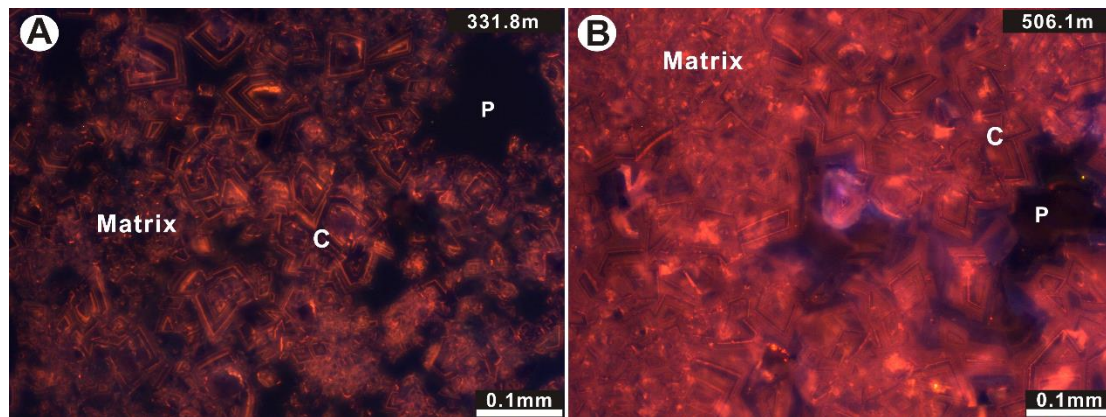


Fig. 8

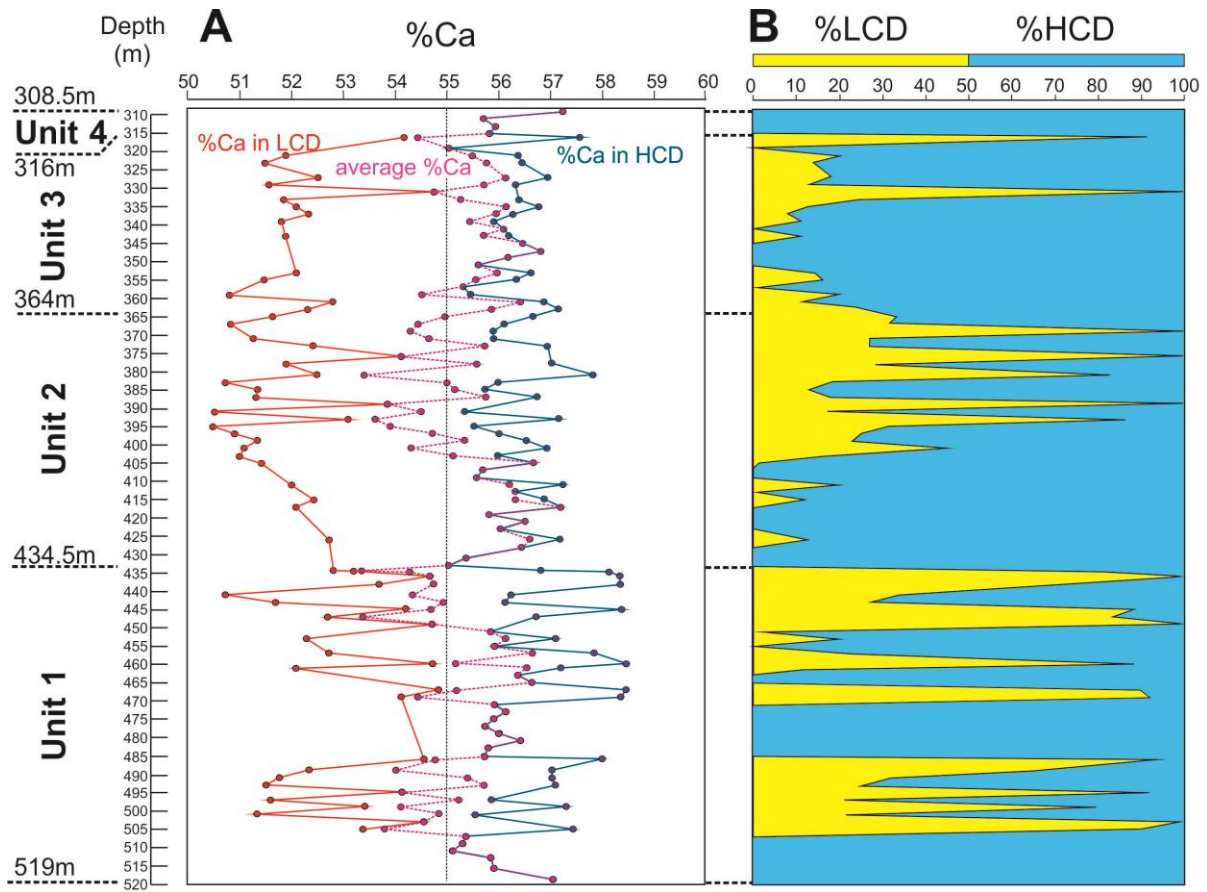


Fig. 9

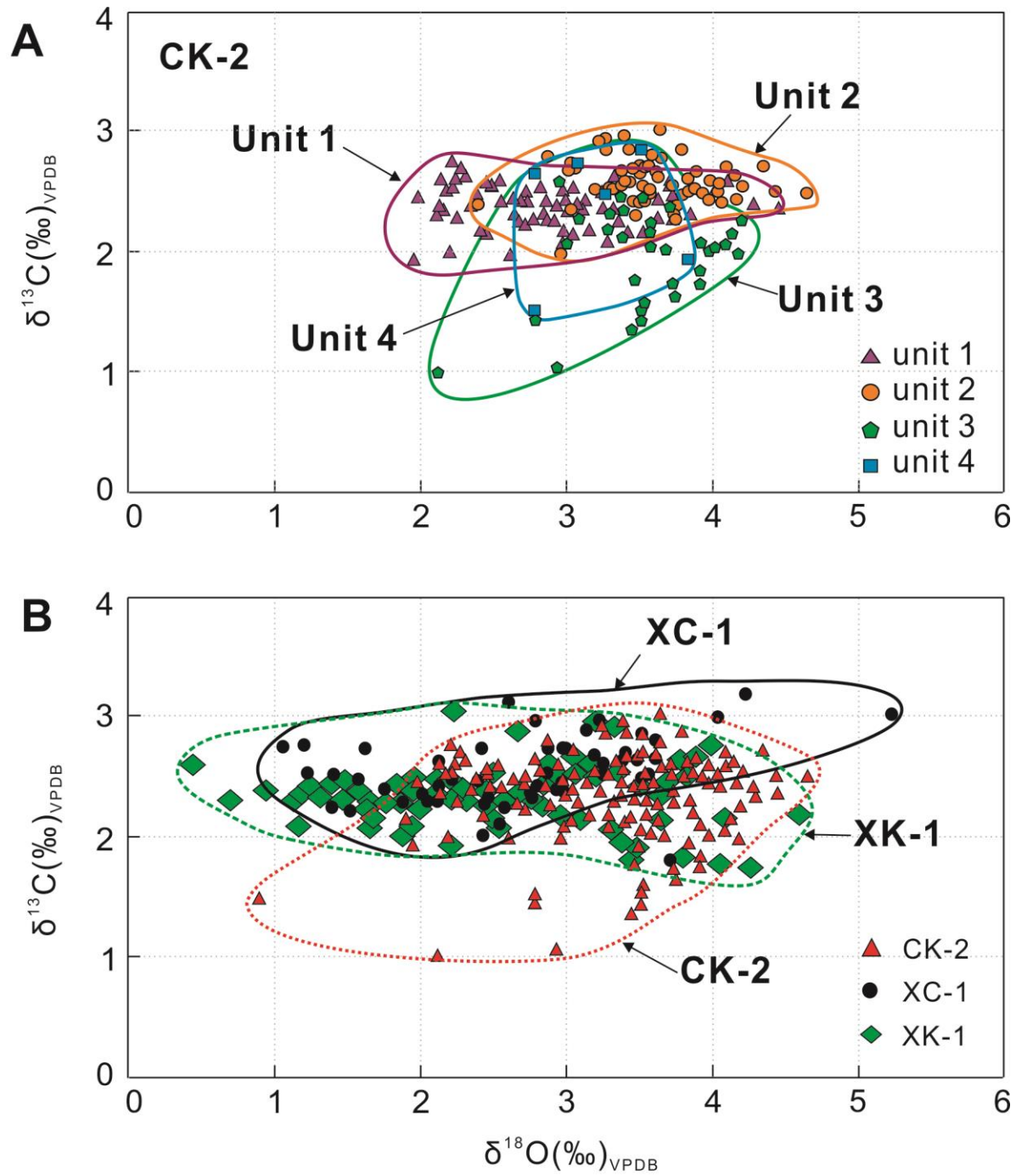


Fig. 10

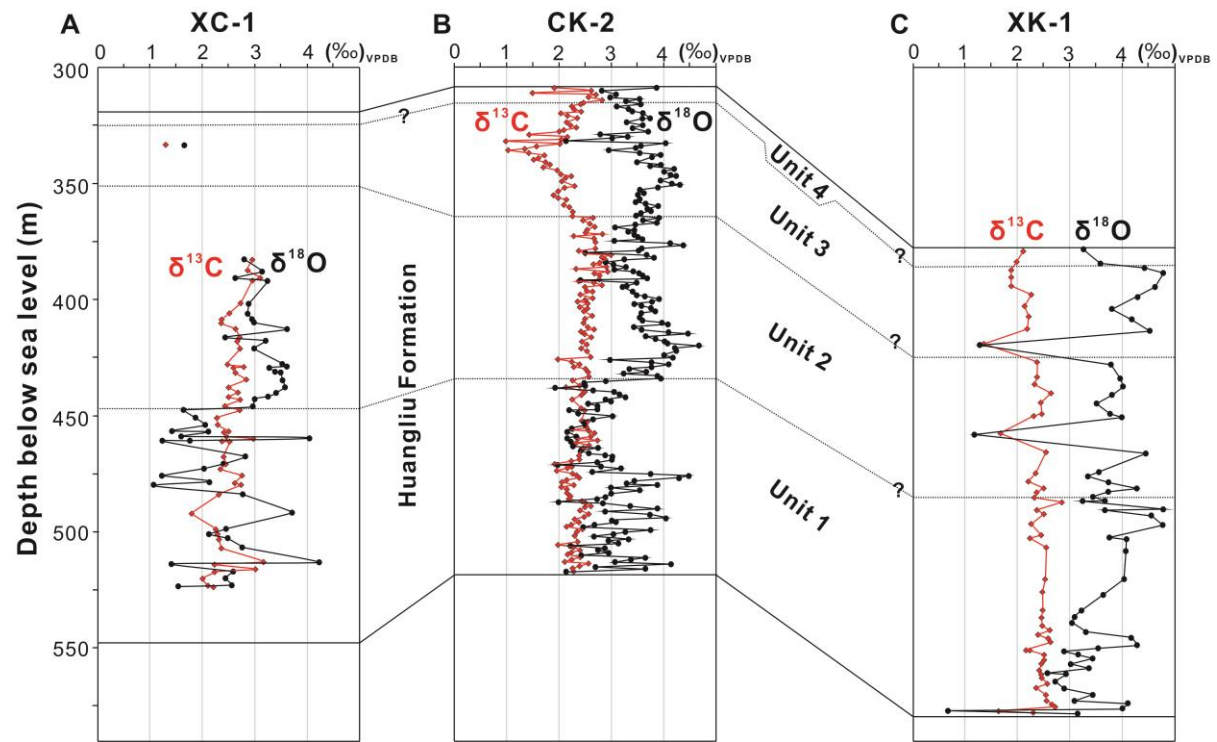


Fig. 11

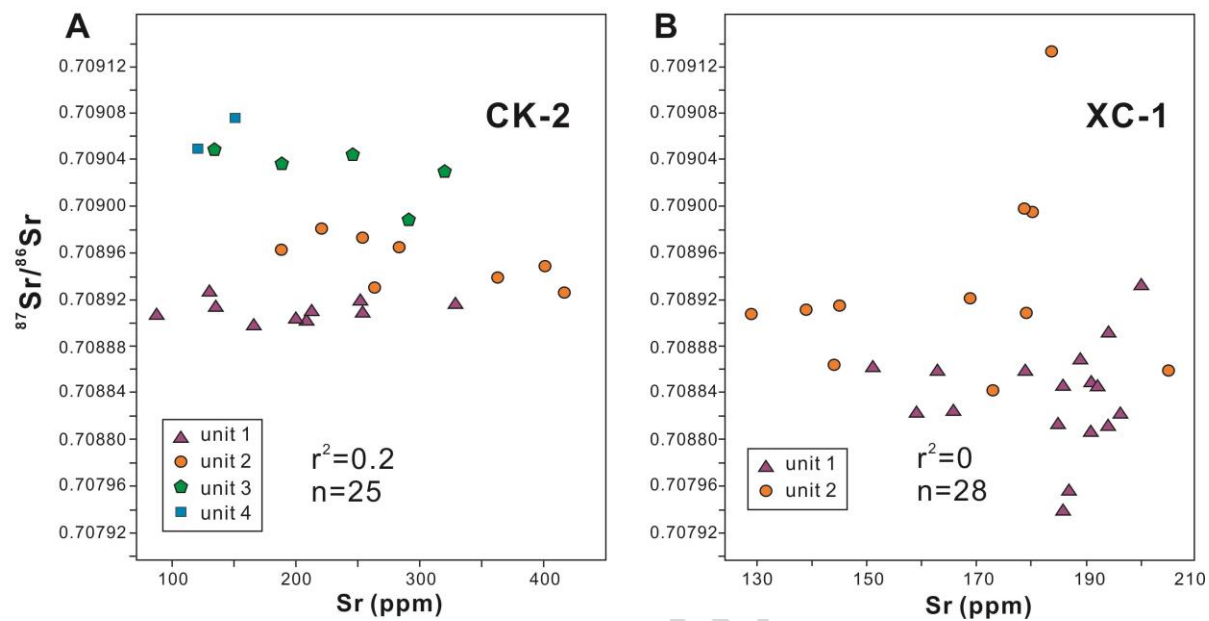


Fig. 12

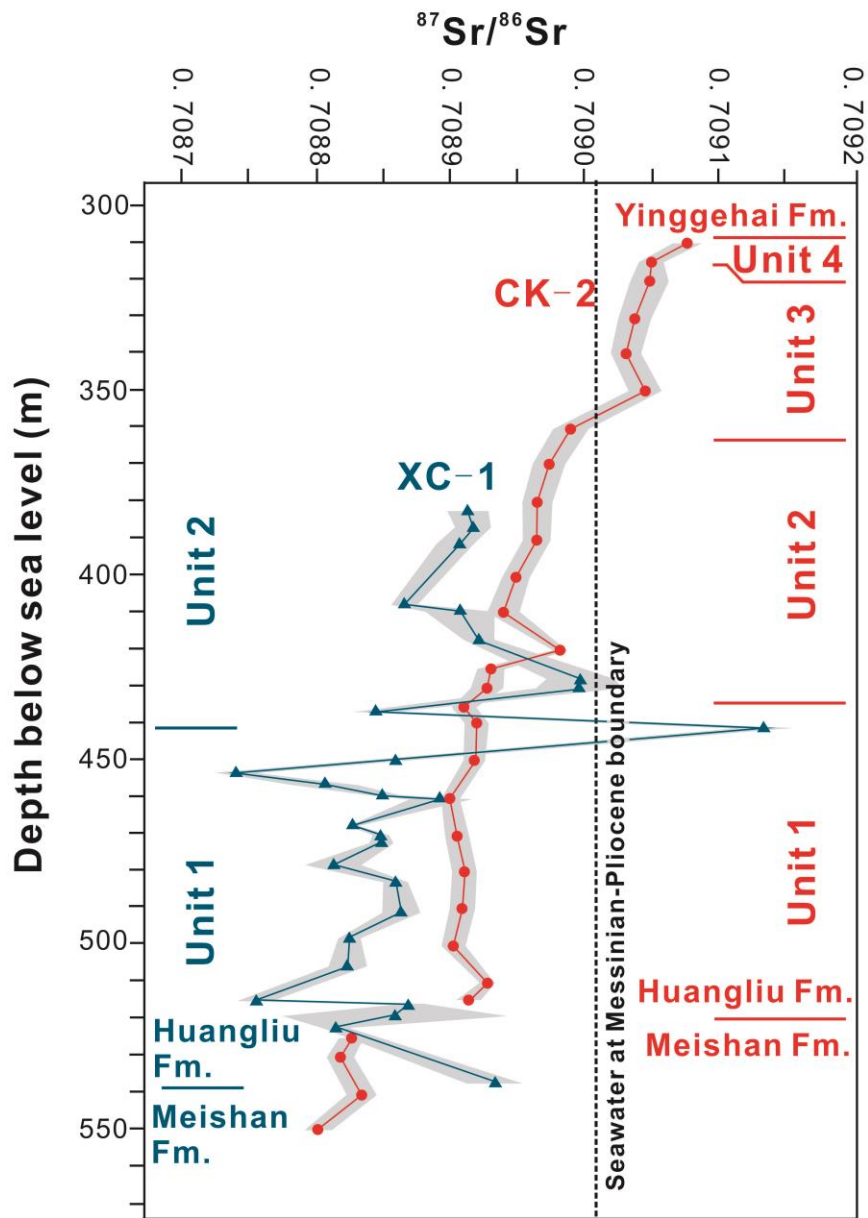


Fig. 13

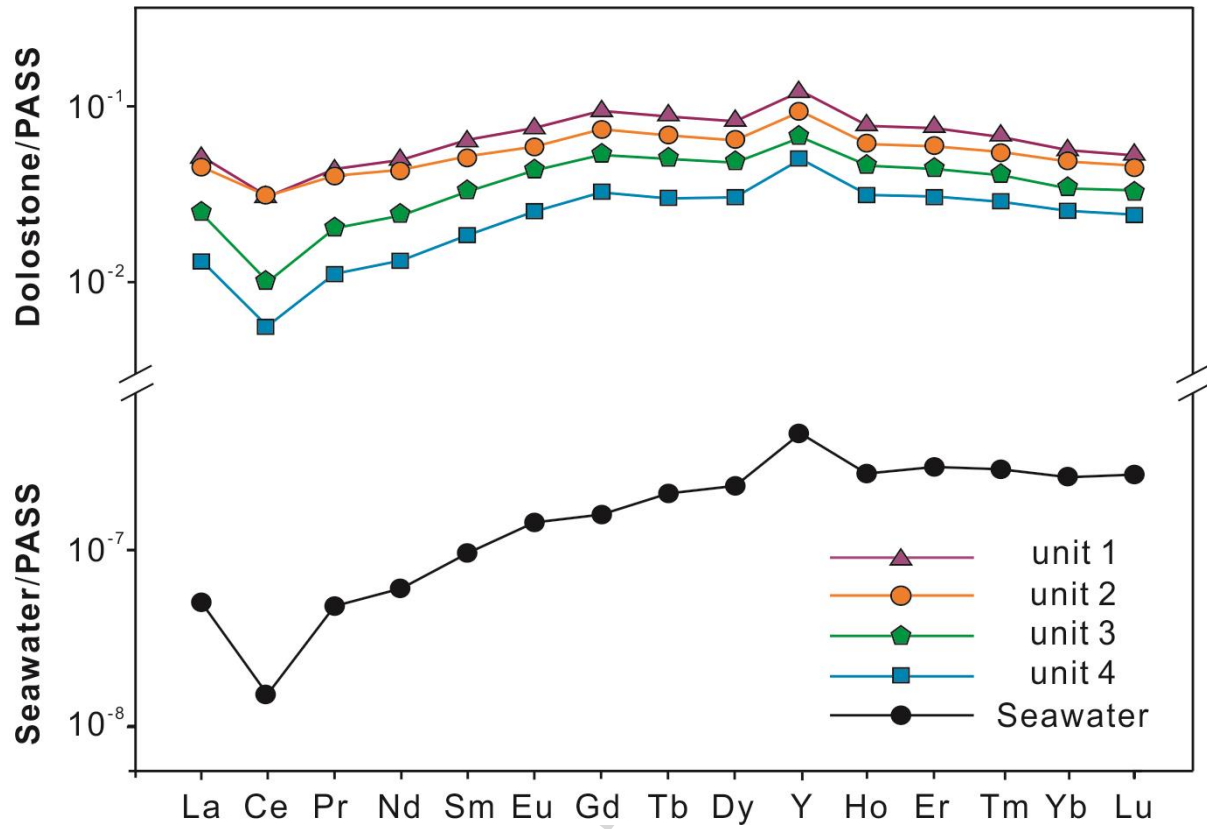


Fig. 14

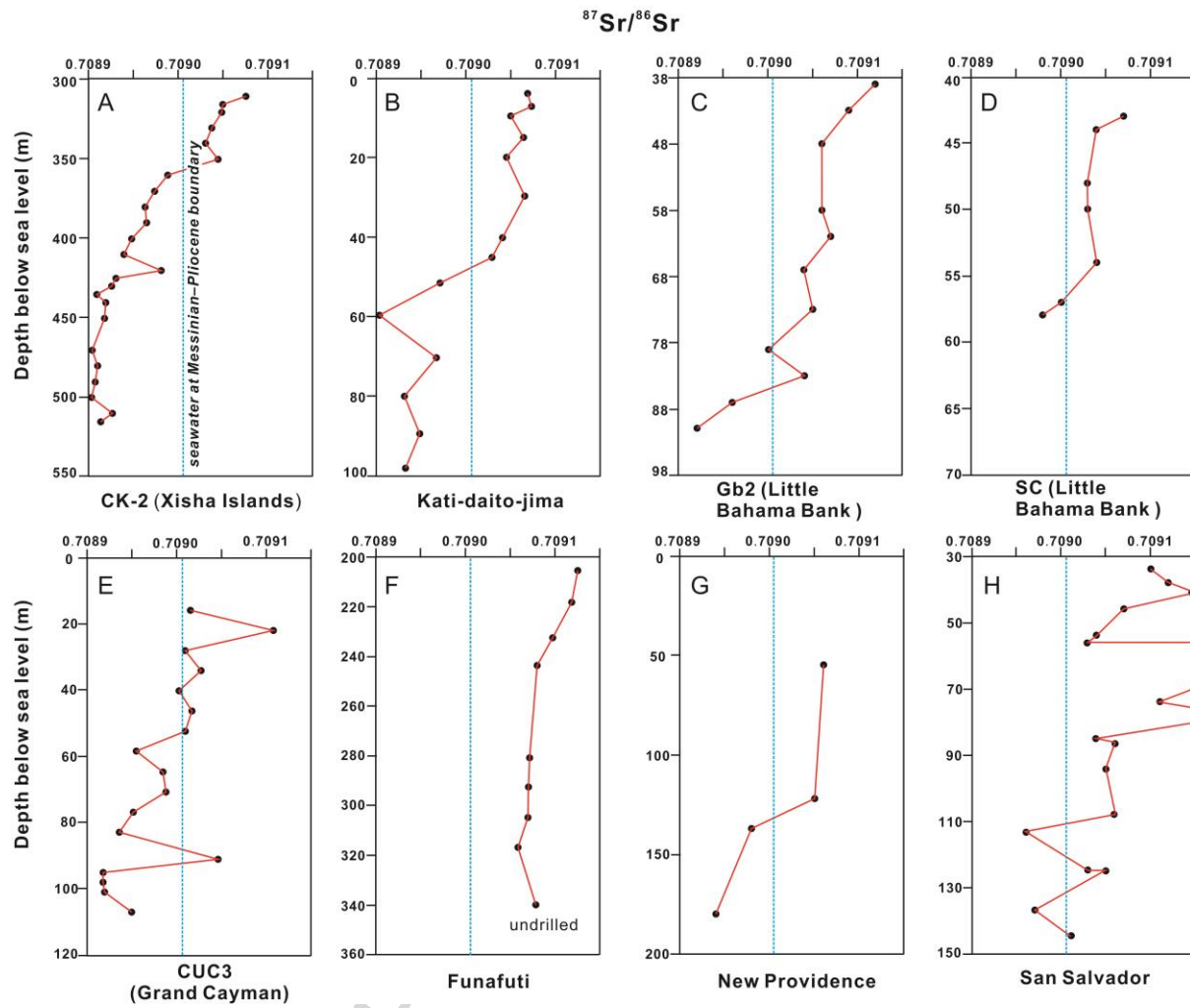


Fig. 15

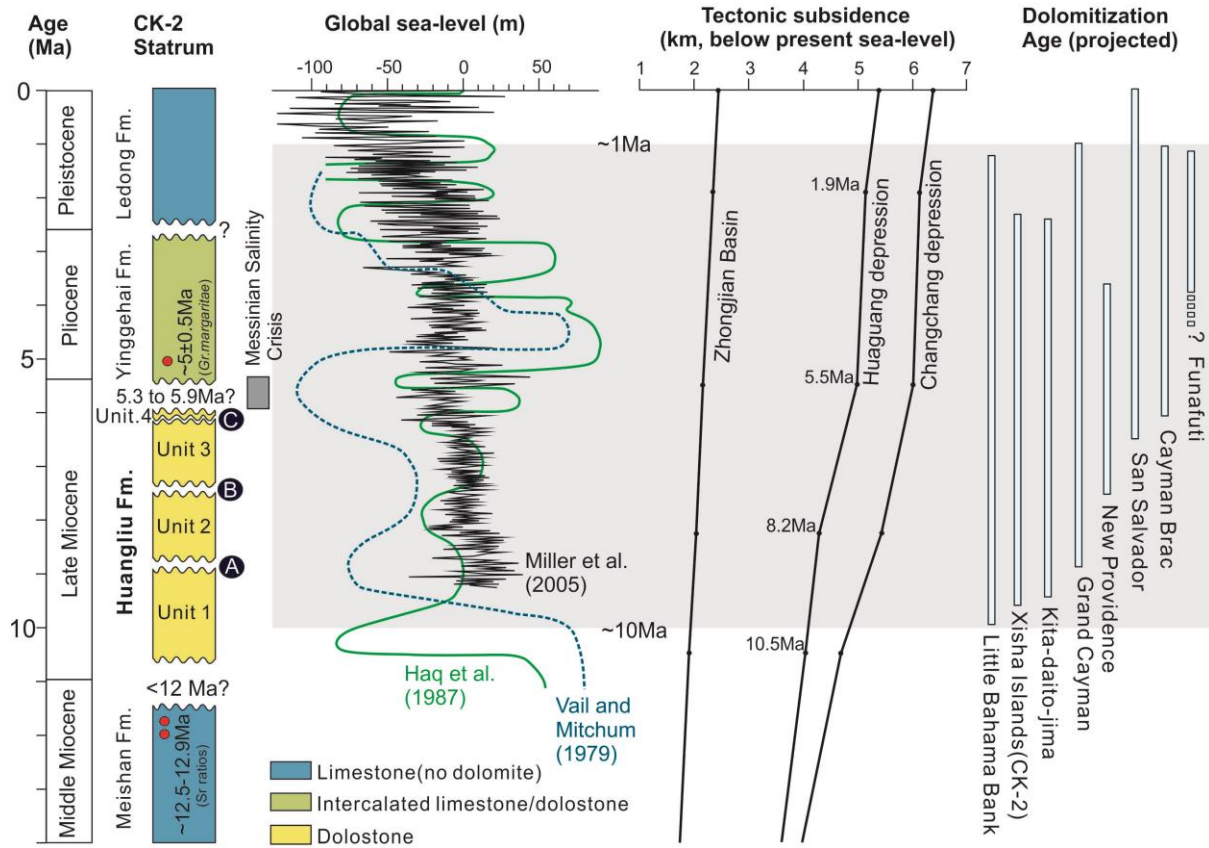


Fig. 16

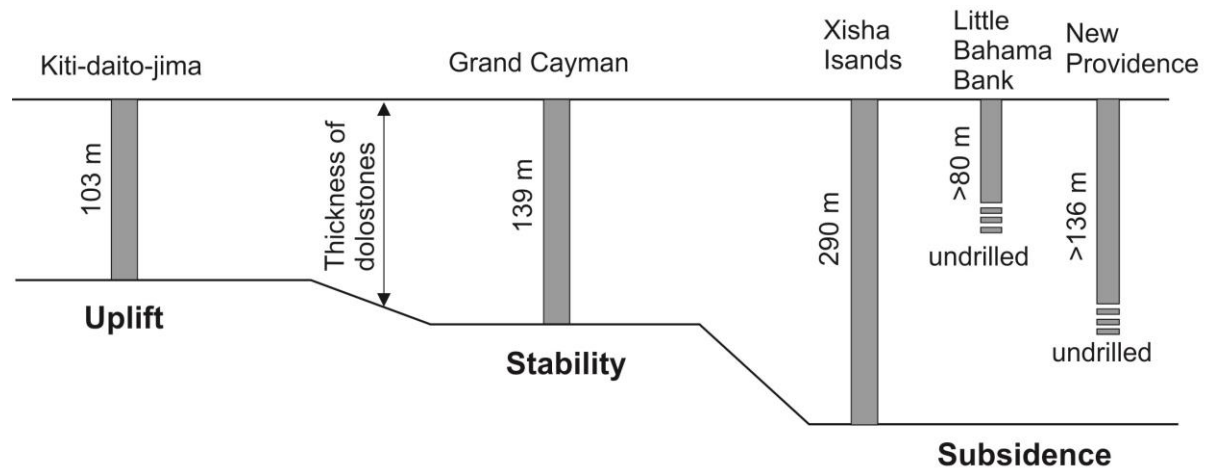


Table 1.

$^{87}\text{Sr}/^{86}\text{Sr}$ ratios and Sr contents for dolostones from the Huangliu Formation in wells CK-2 and XC-1. Data for well XC-1 are from Wei et al. (2007, their Table 1). Depths are below modern sea-level.

Well CK-2					Well XC-1				
Unit	Depth(m)	$^{87}\text{Sr}/^{86}\text{Sr}$	2s	Sr(ppm)	Unit	Depth(m)	$^{87}\text{Sr}/^{86}\text{Sr}$	2s	Sr(ppm)
Unit 4	311	0.709075	0.000011	151		383	0.708912	0.000015	139
	316	0.709049	0.000009	122		388	0.708916	0.000013	145
	321	0.709048	0.000014	134		392	0.708907	0.000011	129
	331	0.709037	0.000012	188		409	0.708865	0.000010	144
	341	0.709030	0.000011	320		410	0.708907	0.000026	179
Unit 3	351	0.709044	0.000012	247		418	0.708920	0.000011	169
	361	0.708988	0.000013	291		429	0.708996	0.000025	179
	371	0.708973	0.000012	254		431	0.708995	0.000032	180
	381	0.708963	0.000011	189		438	0.708844	0.000018	173
	391	0.708964	0.000010	284		442	0.709133	0.000023	184
Unit 2	401	0.708948	0.000010	402	Unit 2	451	0.708859	0.000012	205
	411	0.708939	0.000012	364		454	0.708740	0.000015	186
	421	0.708981	0.000007	221		457	0.708806	0.000024	191
	426	0.708930	0.000010	264		460	0.708849	0.000013	191
	431	0.708926	0.000012	417		461	0.708892	0.000023	194
	436	0.708909	0.000009	255		468	0.708826	0.000003	166
	441	0.708919	0.000009	253		471	0.708847	0.000006	186
	451	0.708917	0.000008	329		473	0.708847	0.000009	192
	461	0.708898	0.000007	166		479	0.708813	0.000021	194
	471	0.708904	0.000009	200		484	0.708859	0.000009	163
	481	0.708910	0.000009	213		492	0.708863	0.000014	151
	491	0.708907	0.000009	88		499	0.708824	0.000008	159
	501	0.708902	0.000009	209		507	0.708823	0.000014	196
	511	0.708926	0.000007	131		516	0.708755	0.000014	187
	Unit 1	516	0.708913	0.000009	136		517	0.708868	0.000012
526		0.708826	0.000009	322		520	0.708859	0.000084	179
531		0.708817	0.000010	298		523	0.708814	0.000010	185
MeiShan Fm.	541	0.708834	0.000011	550	Unit 1	538	0.708933	0.000021	200
	551	0.708800	0.000010	756					

Table 2.Summary of $^{87}\text{Sr}/^{86}\text{Sr}$ ratios values for Cenozoic island dolostones.

Island	Extent of dolomitization*	Formation/ dolomite strata	No. of samples	Sr ratios		Dolomitization Age (Ma)	Data source
				Ranges	Average (2s)		
Xisha	regional	Huangliu Fm.	25	0.708898 to 0.709075	0.708960 (\pm 0.00001)	9.6 to 2.3	Well CK-2
Funafuti	regional	-	9	> 0.709058 to 0.709125	0.709607 (\pm 0.00009)	> 3.8 to 1.2	Shigeru et al. (2002)
Kita-daito-jima	regional	-	14	0.708903 to 0.709073	0.709006 (\pm 0.00002)	9.4 to 2.4	Ohde and Elderfield, (1992)
Niue	localized	upper dolomite	5	0.70912 to 0.70916	0.70914 (\pm 0.00009)	1.3 to 0.5	Aharon et al. (1987)
Little Bahamas Bank	regional	Lower and Upper dolomite	44	0.70889 to 0.70912	0.70903	9.9 to 1.3	Vahrenkamp et al. (1991)
San Salvador	regional	-	23	0.70851 to 0.70863; 0.70896 to 0.70922	0.70904	19 to 17.6; 6.6 to 0	Vahrenkamp et al. (1991)
New Providence	localized	-	4	0.70894 to 0.70906	0.70901	7.3 to 3.6	Vahrenkamp et al. (1991)
Grand Cayman	regional	Pedro Castle Fm., Cayman Fm., Brac Fm.	152	0.708917 to 0.709139	0.709022 (\pm 0.00001)	8.8 to 1	Jones and Luth (2003)
Cayman Brac	regional	Cayman Fm.	45	0.708982 to 0.709132	0.709062 (\pm 0.00001)	6.1 to 1.1	Zhao (2013)
Curacao	localized	Seroe Domi Fm.	21	0.708829 to 0.709010	0.708923 (\pm 0.00002)	12.4 to 5.7	Fouke et al. (1994)

*Extent of dolomitization was referenced by Ren and Jones (2018). Regional dolostones are formed largely of dolostone and geographically cover at least half of the island. Localized dolostone are stratigraphically and geographically restricted, and typically cover less than half of the island. The dolomitization age of Sr ratios was based on the look-up tables from McArthur et al. (2012).

Highlights:

1. The dolostones on Xisha Islands, which took place ~9.4 to 2.3 Ma, appears to have been a (semi-)continuous time-transgressive process. Critically, the same pattern is event in the dolostones from many different Cenozoic islands (e.g. Grand Cayman, Cayman Brac, Kita-daito-jima, Little Bahama Bank, San Salvador) - implying a worldwide phenomenon should be responsible.
2. As for Xisha Islands, this dolomitization process was obviously affected by subsidence. Thus, it probably suggests that, when we used to consider the eustatic changes in sea-level was responsible for the global dolomitization on Cenozoic islands, tectonic factors should be also taken to the consideration.